

RA-DCA: A Randomized Active-Set DCA for Directional Stationarity in Max-Structured DC Programs

Yi-Shuai Niu

Beijing Institute of Mathematical Sciences and Applications (BIMSA), Beijing, China

niuyishuai@bimsa.cn

ORCID: 0000-0002-9993-3681

Abstract

We study nonsmooth difference-of-convex programs whose subtracted convex term is a finite maximum of smooth convex functions. In this setting, standard DCA iterations may converge to critical points that are not directionally stationary, whereas exact active-vertex screening can be expensive when active sets are large or combinatorial. We propose RA-DCA, a vertex-first randomized active-set DCA that projects active gradients onto sampled directions, checks a sampled vertex residual, and uses a small linear program only as a low-residual convex-combination fallback. The method preserves the descent structure of DCA and reduces the randomized screening layer to matrix multiplications. Under the stated regularity, numerical active-set consistency, and random-embedding assumptions, every accumulation point generated by the safeguarded method is directionally stationary with probability one. MATLAB experiments first test the theorem on degenerate max-affine, max-quadratic, and sparse support-function models, where the safeguard avoids nonstationary critical points and closely tracks a full active-vertex scan. Block top-k tests then show that the same screening idea remains useful when exact aggregate enumeration is combinatorial. Trimmed-regression, complementarity, and QUBO diagnostics separate cases where active-set selection helps from cases dominated by multistart search, the DC split, or other problem-specific features.

Keywords: RA-DCA, max-structured DC programming, randomized active-set methods, directional stationarity, nonsmooth nonconvex optimization

MSC2020 subject classifications. 90C26, 90C30, 65K05, 49J52, 68W20, 90C11, 90C33

1 Introduction

1.1 Motivation and contributions

Difference-of-convex (DC) programming is a standard modelling framework for nonconvex optimization [15, 19, 20]. In its simplest unconstrained form one minimizes

$$F(x) := g(x) - h(x), \quad x \in \mathbb{R}^n, \quad (1)$$

where both g and h are convex. The DCA of Pham-Le Thi [31, 20] linearizes h at the current iterate and solves one convex subproblem. This gives a robust and inexpensive algorithm, but its natural limiting condition is criticality, $\partial g(\bar{x}) \cap \partial h(\bar{x}) \neq \emptyset$, which can be weaker than directional stationarity for nonsmooth DC objectives [29].

This paper focuses on the structured case

$$h(x) = \max_{i \in \mathcal{I}} \psi_i(x), \tag{2}$$

where $\mathcal{I} = \{1, \dots, q\}$ is finite and each ψ_i is smooth and convex. This is also the basic block in finite sum-of-max models of the form

$$g(x) = \sum_{\ell=1}^p \max_{i \in \mathcal{I}_\ell} \psi_{\ell i}(x).$$

The single-max case isolates the active-set phenomenon without the additional Cartesian product of block active sets. Finite sums of such blocks are treated through aggregate active vertices after the single-block analysis. Max and sum-of-max structures appear in sparse and trimmed estimation [2, 7], piecewise-affine models [24], exact penalties for complementarity-type constraints [23, 11], and robust optimization [5, 6]. They also expose the limitation of choosing an active subgradient without checking the active vertices. At a point where several ψ_i are active, one vertex of the active subdifferential may give a useful descent step while an averaged subgradient may satisfy the weaker criticality condition and stop at a point that has an immediate descent direction. Section 2 makes this distinction precise and gives a one-dimensional example before the algorithm is introduced.

Several enhanced DC methods address this issue by considering active pieces separately. Examples include the algorithmic framework of Pang et al. [29], decomposition and statistical difference-max extensions [30, 10], and enhanced proximal variants [22] and [21]. Single-active-piece heuristics reduce some per-iteration costs, but their practical behaviour is still tied to which active piece is selected. In independent recent work, Le Thi, Huynh, and Pham Dinh [17] proposed a unified DCA-type framework for computing directional stationary points of broad classes of DC programs, covering finite- and infinite-maximum representations of the subtracted convex component and, more generally, continuous convex components. Their contribution is a general convergence framework based on solving selected convex subproblems; its randomized variant samples components to reduce the number of subproblems. By contrast, the present paper takes a more specialized and computational viewpoint: it focuses on finite max-structured and sum-of-max DC models and uses randomized active-set screening based on vertex residuals, random projections, and a convex-combination LP fallback. Section 6 tests this active-set selection mechanism in large or combinatorial active sets. The question motivating RA-DCA is whether randomized directions can summarize the active subdifferential computationally while still safeguarding the stronger directional-stationarity condition.

Our contribution is a vertex-first randomized active-set DCA. The method projects active gradients onto randomly sampled directions and first evaluates a sampled vertex residual. If this residual is large, RA-DCA takes the most violating active vertex; only in the low-residual regime does it solve a small linear program for convex-combination weights over the active set. This ordering is deliberate: the linear program is a centering mechanism for DCA criticality, whereas the vertex residual is the directional-stationarity safeguard that prevents accepting a merely averaged criticality certificate.

The resulting method has a simple computational kernel: its main additional cost is forming products between a random direction matrix and an active-gradient matrix. This structure can be vectorized and is the basis for the reported numerical implementation. The main convergence theorem is proved for the single finite maximum; the exact block corollary records what must be safeguarded when finite sums of max terms are handled through aggregate active vertices. A supporting worst-iterate residual bound is proved in Appendix A; it gives stationarity-complexity context without changing the main asymptotic theorem.

The computational claims are correspondingly specific. RA-DCA targets iterations at which several active pieces compete and an averaged active subgradient can hide a descent direction. In smooth portions of a trajectory, or in problems where multistart exploration is the dominant issue, the randomized active-set rule need not be the limiting factor. The numerical section therefore separates direct tests of the theorem from block aggregate tests and boundary penalty diagnostics, so that performance gains are interpreted relative to the amount of active-set ambiguity present.

1.2 Model classes and applications

The finite-max model (2) is structured enough to permit a clean active-set theory, but broad enough to cover several useful DC constructions. Several model classes clarify what is covered directly by the present paper and what is treated through the block extension.

Piecewise-affine and robust losses. If

$$h(x) = \max_{i \in \mathcal{I}} (a_i^\top x + b_i),$$

then $\partial h(x)$ is exactly the convex hull of the active affine gradients. This includes max-affine penalties, worst-case linear models, polyhedral robust losses, and the signed-pair instances used in Section 6; see, for example, [24, 5, 6]. RA-DCA applies directly, and the randomized projection step reduces to products between the sampled direction matrix and the active gradient matrix.

Smooth finite maxima. The same framework applies when the pieces are smooth convex functions, for example

$$h(x) = \max_i \{a_i^\top x + \frac{\gamma_i}{2} \|x\|^2\} \quad \text{or} \quad h(x) = \max_i \psi_i(x).$$

The active gradients now change with x , but the active subdifferential is still the convex hull in (3). The max-quadratic tests in Section 6 are included to check this non-affine case; the basic finite-maximum calculus follows standard convex analysis [33, 9].

Sparse and trimmed optimization. Several feature-selection and robust-estimation penalties use order statistics or top- k terms [2, 7]. For example, top- k absolute-value terms can be written as the maximum over subsets of size k ,

$$\|x\|_{(k)} = \max_{\substack{S \subseteq \{1, \dots, n\} \\ |S|=k}} \sum_{i \in S} |x_i|.$$

After the usual smoothing or sign-pattern treatment away from zero, the active sets correspond to tied top- k subsets. RA-DCA is relevant here because ties produce many active gradients and averaged choices can be weak. Large-scale implementations would need implicit active-set generation rather than explicit enumeration of all subsets.

Complementarity and infeasibility penalties. For a linear complementarity system of the form

$$0 \leq x \perp Mx + q \geq 0,$$

violations of nonnegativity can be penalized by terms such as

$$\max\{-x_i, -(Mx + q)_i, 0\}.$$

Such penalties are max-affine locally and therefore have exactly the active-set structure exploited by RA-DCA. Exact penalty and nonlinear programming treatments of complementarity constraints are classical in MPEC and LCP computation [23, 11]. A full complementarity merit function typically contains a sum of these max terms and possibly a product-type complementarity penalty. Thus a

single max block is covered directly by the main theorem, while a complete LCP penalty model belongs to the block viewpoint formalized in Section 4.4. Section 6.9 uses the box-complementarity case $0 \leq x_i \perp 1 - x_i \geq 0$ to motivate a less symmetric block test.

Integer and mixed-integer penalties. Binary restrictions $y_i \in \{0, 1\}$ are often relaxed with penalties such as $y_i(1 - y_i)$ on $0 \leq y_i \leq 1$, or with piecewise-linear penalties for distance to $\{0, 1\}$. These formulations are naturally DC and can contain max-affine pieces. They connect with algebraic DC decompositions of polynomials [1, 27] and with DC cutting-plane approaches for mixed-binary linear programs [28]; related sparse and binary optimization models are discussed in [7]. They are promising applications for active-set DCA because many binary variables can become nearly tied near fractional values. Unconstrained binary quadratic programming is a particularly convenient test case [4] because the quadratic part can be split as $Q = Q_+ - Q_-$ with $Q_{\pm} \succeq 0$, while the binary penalty supplies the max blocks. Boolean-polynomial dynamical-system methods have also used Max-Cut and QUBO benchmarks to test continuous relaxations of binary polynomial models [26]. However, the most useful mixed-integer penalty models generally combine many blocks and additional constraints. They are computational block extensions of the single-max analysis, whereas the main theorem covers the single-block case.

Clustering and sum-of-max models. DC formulations of assignment-type clustering or k -median often contain a sum of max terms, one for each data point [18, 3]. The active set then has a product or block structure. The present algorithmic idea extends naturally: construct active gradients blockwise, sketch the aggregate active-gradient matrix, and safeguard vertices or block vertices. Section 4.4 records the corresponding residual and explains how the single-max analysis extends when the aggregate active vertices are checked. Clustering requires application-specific subproblem solvers and data structures, and is therefore outside the present computational scope.

These examples motivate the current focus on (2). It is the basic active-set block that appears inside more elaborate sparse, complementarity, mixed-integer, and clustering models. The paper therefore separates the analysis into a single-block theory and an exact aggregate-vertex corollary for finite block sums, with computational block experiments used to illustrate the latter block viewpoint rather than extend the theorem.

1.3 Organization

Section 2 formalizes the finite-max DC model and distinguishes criticality from directional stationarity. Section 3 introduces RA-DCA, including the vertex-first safeguard and the convex-combination LP fallback. Section 4 proves descent, almost-sure directional stationarity, and the exact block extension. Section 5 records the implementation choices relevant to reproducibility. Section 6 reports the MATLAB experiments, and Section 7 closes the main text. The appendices contain supporting material rather than additional main claims: Appendix A gives a worst-iterate residual bound, Appendix B records the approximate block safeguard and the numerical-active-set variants, Appendix C gives the additional QUBO diagnostics, and Appendix D reports the LP and safeguard diagnostics.

2 Problem class and stationarity

For $x \in \mathbb{R}^n$, define the active index set

$$\mathcal{A}(x) := \{i \in \mathcal{I} : \psi_i(x) = h(x)\}.$$

Since h is a finite maximum of smooth convex functions,

$$\partial h(x) = \text{conv}\{\nabla \psi_i(x) : i \in \mathcal{A}(x)\}. \quad (3)$$

When g is differentiable, the classical DCA criticality condition is

$$\nabla g(x) \in \partial h(x). \quad (4)$$

By contrast, x is directional-stationary for (1) if

$$F'(x; d) = \langle \nabla g(x), d \rangle - \max_{i \in \mathcal{A}(x)} \langle \nabla \psi_i(x), d \rangle \geq 0 \quad \text{for all } d \in \mathbb{R}^n. \quad (5)$$

The following residual is useful both theoretically and computationally:

$$R_d(x) := \max_{i \in \mathcal{A}(x)} \|\nabla g(x) - \nabla \psi_i(x)\|. \quad (6)$$

Lemma 2.1. *For (1)–(2), x is directional-stationary if and only if $R_d(x) = 0$. The residual also controls the convex criticality residual:*

$$\text{dist}(\nabla g(x), \partial h(x)) \leq R_d(x),$$

and the inequality can be strict.

Proof. Condition (5) is equivalent to

$$\langle \nabla g(x), d \rangle \geq \max_{i \in \mathcal{A}(x)} \langle \nabla \psi_i(x), d \rangle \quad \text{for all } d \in \mathbb{R}^n.$$

The maximum is no larger than the left-hand side if and only if every active linear form is no larger than the left-hand side. Hence this is equivalent to

$$\langle \nabla g(x) - \nabla \psi_i(x), d \rangle \geq 0 \quad \text{for all } d \in \mathbb{R}^n, i \in \mathcal{A}(x).$$

Fix an active index i and set $w_i = \nabla g(x) - \nabla \psi_i(x)$. Since the last inequality holds for every direction d , it holds in particular for $d = -w_i$, giving $- \|w_i\|^2 \geq 0$. Thus $w_i = 0$, and $\nabla g(x) = \nabla \psi_i(x)$ for every active i . This is precisely $R_d(x) = 0$. Conversely, if $R_d(x) = 0$, then all active gradients equal $\nabla g(x)$, so

$$\max_{i \in \mathcal{A}(x)} \langle \nabla \psi_i(x), d \rangle = \langle \nabla g(x), d \rangle \quad \text{for all } d,$$

and (5) follows.

For the distance estimate, (3) shows that each active gradient $\nabla \psi_i(x)$ belongs to $\partial h(x)$. Therefore

$$\text{dist}(\nabla g(x), \partial h(x)) \leq \min_{i \in \mathcal{A}(x)} \|\nabla g(x) - \nabla \psi_i(x)\| \leq R_d(x).$$

Strictness is demonstrated by Example 2.2. □

Example 2.2 (A one-dimensional nonstationary critical point). Let $g(x) = \frac{1}{2}x^2$ and $h(x) = \max\{x, -x\} = |x|$. Then

$$F(x) = \frac{1}{2}x^2 - |x| = \frac{1}{2}(|x| - 1)^2 - \frac{1}{2}.$$

At $x = 0$, $\nabla g(0) = 0$ and $\partial h(0) = [-1, 1]$. Hence $0 \in \partial h(0)$, so $x = 0$ is a DCA critical point and $\text{dist}(\nabla g(0), \partial h(0)) = 0$. It is not directional-stationary, because the active gradients are 1 and -1 , and $R_d(0) = 1$. Equivalently, $F'(0; d) = -|d| < 0$ for every $d \neq 0$.

By contrast, $x = 1$ and $x = -1$ are single-active points satisfying $\nabla g(1) = 1 = \nabla x$ and $\nabla g(-1) = -1 = \nabla(-x)$. Thus both points are directional-stationary; they are also the global minimizers. If traditional DCA uses the centered subgradient $v = 0 \in \partial h(0)$, then its subproblem gives $x^+ = v = 0$, so the method can remain at the non-directional-stationary critical point. Choosing an extreme active gradient instead moves the iterate to one of the two directional-stationary minimizers.

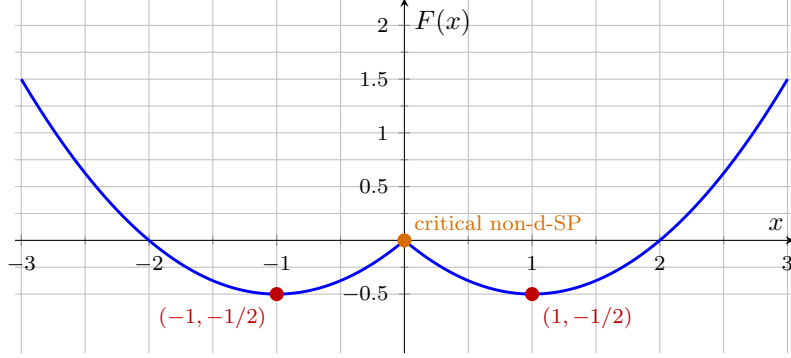


Figure 1: The one-dimensional nonstationary critical point in Example 2.2: $x = 0$ is a DCA critical point but is not directional-stationary, while $x = \pm 1$ are directional-stationary global minimizers.

Lemma 2.1 is the key structural distinction used by RA-DCA. The criticality test asks whether $\nabla g(x)$ lies in the convex hull of the active gradients. Directional stationarity asks for more: every active vertex must give the same first-order response as $\nabla g(x)$. Thus an averaged active subgradient may be a valid DCA certificate while still hiding a descent direction exposed by an extreme active gradient. RA-DCA separates these two tasks: a convex combination is used for stable centering, while a vertex-level residual provides the stationarity safeguard. The condition is not vacuous: at points with a single active piece it reduces to the usual smooth stationarity equation $\nabla g(x) = \nabla \psi_i(x)$. At a genuine nonsmooth tie with different active gradients, however, directional stationarity is possible only if those gradients all agree with $\nabla g(x)$. This is exactly the point: for an unconstrained objective $g - \max_i \psi_i$, a nonzero active-gradient spread creates a feasible descent direction, so a convex-hull criticality certificate is not enough.

3 The RA-DCA algorithm

RA-DCA is a randomized active-set DCA method that keeps the usual convex DCA subproblem while replacing a deterministic active-gradient choice by a vertex-first randomized active-set calculation. The convex-combination LP is retained as a centering fallback, but it is called only after the sampled vertex residual is below the safeguard threshold. At iteration k , the method first forms the numerical active set

$$\mathcal{A}_k = \{i \in \mathcal{I} : h(x^k) - \psi_i(x^k) \leq \varepsilon_k\},$$

where $\varepsilon_k \geq 0$ is a numerical active-set tolerance. Let

$$G_k = [\nabla \psi_i(x^k)]_{i \in \mathcal{A}_k} \in \mathbb{R}^{n \times r_k}, \quad r_k = |\mathcal{A}_k|,$$

and let $g_k = \nabla g(x^k)$. A random direction matrix $D_k \in \mathbb{R}^{m_k \times n}$ is generated by sampling rows uniformly on the unit sphere and scaling by $\sqrt{n/m_k}$, or equivalently by using Gaussian rows with variance $1/m_k$. Thus $D_k z$ is a randomized sketch of z .

Algorithm 1 summarizes the full iteration in a self-contained form; the subsequent subsections define the safeguard residual, vertex rule, LP fallback, and proximal DCA subproblem.

3.1 Reference active-gradient rules

Algorithm 1 is the proposed method. The numerical section also uses three reference DCA rules that differ only in the way the active linearization vector v^k is chosen; after that choice, they all use

Algorithm 1 RA-DCA

Require: x^0 ; tolerances $\{\varepsilon_k\}, \{\tau_k\}$; sample-size rule for $m_k \in \mathbb{N}$; $\sigma \geq 0$

```
1: for  $k = 0, 1, 2, \dots$  do
2:   Form  $\mathcal{A}_k = \{i : h(x^k) - \psi_i(x^k) \leq \varepsilon_k\}$  and  $G_k = [\nabla\psi_i(x^k)]_{i \in \mathcal{A}_k}$ 
3:   Set  $g_k = \nabla g(x^k)$ 
4:   Choose the number  $m_k$  of sampled directions
5:   Draw  $D_k \in \mathbb{R}^{m_k \times n}$ 
6:   Compute  $\widehat{R}_k = \max_{i \in \mathcal{A}_k} \|D_k(\nabla\psi_i(x^k) - g_k)\|$ 
7:   if  $\widehat{R}_k > \tau_k$  then
8:     Choose  $i_k \in \operatorname{argmax}_{i \in \mathcal{A}_k} \|D_k(\nabla\psi_i(x^k) - g_k)\|$ 
9:     Set  $v^k = \nabla\psi_{i_k}(x^k)$ 
10:  else
11:    Solve the active convex-combination LP for  $\alpha^k$  and set  $v_c^k = G_k\alpha^k$ 
12:    Set  $v^k = v_c^k$ 
13:  end if
14:  Compute  $x^{k+1} = \operatorname{argmin}_x \{g(x) - \langle v^k, x - x^k \rangle + \frac{\sigma}{2} \|x - x^k\|^2\}$ 
15:  if  $\|x^{k+1} - x^k\|$  and the stationarity residual are below the requested tolerances then
16:    Stop
17:  end if
18: end for
```

the same convex update subproblem in Algorithm 1. For the single finite maximum, the rules are as follows. Centered DCA uses the active-gradient average

$$v_{\text{cen}}^k = \frac{1}{r_k} \sum_{i \in \mathcal{A}_k} \nabla\psi_i(x^k).$$

Random-vertex DCA samples a single active piece,

$$v_{\text{rand}}^k = \nabla\psi_{I_k}(x^k), \quad I_k \sim \text{Unif}(\mathcal{A}_k).$$

Full-vertex DCA uses the exact active-set residual scan,

$$v_{\text{full}}^k = \nabla\psi_{i_k}(x^k), \quad i_k \in \operatorname{argmax}_{i \in \mathcal{A}_k} \|\nabla\psi_i(x^k) - g_k\|.$$

Thus centered DCA is a convex-hull based criticality rule. Random-vertex DCA tests the effect of choosing a single active piece. Full-vertex DCA is the exact active-set screening rule when the full residual scan is affordable. RA-DCA can be read as a safeguarded randomized variant: it uses the sketched residual to decide whether to take a violating active vertex, and uses the LP candidate only when this safeguard does not trigger.

3.2 Active convex-combination LP

The fallback used when the vertex safeguard does not trigger is a convex combination of active gradients. For fixed x^k , a DCA step is determined by a linearization vector $v^k \in \partial h(x^k)$. Since h is a finite maximum, this amounts to choosing simplex weights on active gradients:

$$v^k = G_k\alpha, \quad \mathbf{1}^\top \alpha = 1, \quad \alpha \geq 0.$$

The LP (7) is introduced to choose this vector in a way that is consistent with the DCA criticality condition (4). If x^k is critical, then $g_k \in \partial h(x^k)$, so there exists a simplex vector α satisfying $G_k \alpha = g_k$. Using such a vector makes the DCA subproblem locally balanced at x^k , whereas an arbitrary active vertex may generate a spurious move even when DCA criticality already holds. This also identifies the regime in which the LP can have a visible numerical effect. If the vertex residual is large, the safeguard deliberately rejects the convex combination and the LP is not used. Under the embedding condition, when the safeguard does not trigger, all active vertex mismatches are already small in the full space up to the sketching distortion. The LP therefore should not be expected to produce large objective improvements far from stationarity. Its role is local: it stabilizes the DCA step when the active set contains nearly tied pieces, or when an ε_k -active set includes pieces that are inactive for the exact maximum but indistinguishable at the chosen numerical tolerance.

Away from exact criticality, the same idea asks for a convex combination $G_k \alpha$ that is close to g_k . The full-space projection $\min_{\alpha \in \Delta} \|G_k \alpha - g_k\|$ is a simplex-constrained quadratic problem. RA-DCA does not solve this Euclidean projection. Instead it uses a randomized Chebyshev surrogate based on sampled directional derivatives: it requires the mismatch to be small in the ℓ_∞ norm after applying D_k , namely $D_k(G_k \alpha - g_k)$. The two formulations coincide only in special cases, for example if the full-space norm is replaced by ℓ_∞ and the sketch is $D_k = I$. Thus the LP is a centering device for selecting a stable DCA linearization, not a certificate of directional stationarity; the latter is checked by the vertex safeguard.

The formulation therefore chooses $\alpha \in \mathbb{R}^{r_k}$ in the simplex and the smallest scalar t that bounds the sampled directional mismatch in the ℓ_∞ norm:

$$\begin{aligned} \min_{\alpha, t} \quad & t \\ \text{s.t.} \quad & -t\mathbf{1} \leq D_k(G_k \alpha - g_k) \leq t\mathbf{1}, \\ & \mathbf{1}^\top \alpha = 1, \quad \alpha \geq 0, \quad t \geq 0. \end{aligned} \tag{7}$$

The LP has only $r_k + 1$ variables and $2m_k + 1$ affine constraints. Its coefficient matrix is

$$D_k G_k = [\langle d_j, \nabla \psi_i(x^k) \rangle]_{j,i}, \quad D_k g_k = [\langle d_j, \nabla g(x^k) \rangle]_j,$$

which is a matrix-matrix product plus a matrix-vector product. This is the part of the method that can be accelerated directly on a GPU. Except in degenerate cases, such as a singleton active set, this Chebyshev approximation problem over the simplex does not have a useful closed-form solution; it is solved as a small continuous LP.

When the vertex safeguard is not triggered, let α^k solve (7) and define

$$v_c^k = G_k \alpha^k \in \text{conv}\{\nabla \psi_i(x^k) : i \in \mathcal{A}_k\}.$$

This vector is the active convex-combination candidate. It is useful for a stable DCA step, but it is not sufficient for directional stationarity.

3.3 Vertex safeguard

The reason for the safeguard is the distinction in Lemma 2.1. The LP (7) can make a convex combination $G_k \alpha$ close to g_k , which is the right test for DCA criticality. This can nevertheless hide a directional-stationarity violation: different active gradients may cancel in their convex hull even though some active vertex is far from g_k . Directional stationarity rules out this cancellation and requires all active vertices to agree with g_k . The safeguard therefore checks the active vertices themselves.

The sampled directional-stationarity residual is

$$\widehat{R}_k = \max_{i \in \mathcal{A}_k} \left\| D_k(\nabla\psi_i(x^k) - g_k) \right\|. \quad (8)$$

It is a randomized proxy for the vertex residual $R_d(x^k)$. When this residual is large, using the convex-combination candidate v_c^k would risk accepting a merely critical point. RA-DCA instead selects the most violating active vertex, which forces the next DCA subproblem to respond to the detected violation. If the exact residual $R_d(x^k)$ can be scanned cheaply, then the corresponding exact full-vertex rule is natural: choose

$$i_k \in \operatorname{argmax}_{i \in \mathcal{A}_k} \left\| \nabla\psi_i(x^k) - g_k \right\|$$

and set $v^k = \nabla\psi_{i_k}(x^k)$ whenever this maximum is nonzero. This rule is the full-vertex DCA baseline in Section 6, and it is the ideal active-set screening rule in the single finite-maximum case. For an explicit single maximum with all active gradients already materialized, this exact scan costs $O(nr_k)$ and is usually no more expensive than a dense sketched scan; setting $D_k = I$ in the safeguard recovers precisely this full-vertex rule. In such explicit small- or medium-scale cases, the full-vertex scan is the appropriate reference. The randomized safeguard is aimed at settings in which only directional products $D_k G_k$ are formed, when the same projected matrix is reused by the LP, or when the exact aggregate-vertex scan in a sum-of-max model is combinatorial. Moreover, when the sampled residual is already below τ_k , the identity of the largest sketched vertex is no longer a robust stationarity signal; a convex-combination step is then used as a stable DCA centering step. The convergence proof uses $\tau_k \downarrow 0$, so this LP branch can persist near an accumulation point only when the exact vertex residual is also small. If \widehat{R}_k is larger than a tolerance τ_k , RA-DCA selects the most violating active vertex

$$i_k \in \operatorname{argmax}_{i \in \mathcal{A}_k} \left\| D_k(\nabla\psi_i(x^k) - g_k) \right\| \quad (9)$$

and sets $v^k = \nabla\psi_{i_k}(x^k)$. In this case the LP (7) is not needed. Otherwise RA-DCA solves (7) and sets $v^k = v_c^k$. This ordering is computationally important for large active sets: the LP is used only when the sampled vertex residual is already below the safeguard tolerance. The next iterate is the proximal DCA point

$$x^{k+1} = \operatorname{argmin}_x \left\{ g(x) - \langle v^k, x - x^k \rangle + \frac{\sigma}{2} \|x - x^k\|^2 \right\}. \quad (10)$$

When g is already strongly convex, σ may be set to zero. Otherwise $\sigma > 0$ makes (10) strongly convex and controls the step. Under this condition the minimizer in (10) is unique. The integer m_k is the number of sampled directions at iteration k . It may be fixed in advance or chosen from the active set after G_k is formed; the embedding-based choice used in the analysis is given in (15).

The two tolerances have different roles. The parameter ε_k defines the numerical active set. It should be large enough to include pieces that are tied up to evaluation error, but small enough that inactive pieces do not dominate the DCA linearization. The convergence analysis assumes a summable sequence, for instance $\varepsilon_k = \varepsilon_0/(k+1)^{1+\beta}$ with $\beta > 0$. The parameter τ_k is the safeguard threshold: values above τ_k force an active vertex step, while values below τ_k allow the LP-centered step. The almost-sure result requires $\tau_k \downarrow 0$, and the residual bound in Appendix A shows that $\tau_k = O((k+1)^{-1/2})$, or a faster decay, is consistent with the $O(k^{-1/2})$ worst-iterate stationarity scale. In finite-precision experiments we use fixed machine-level active-set and safeguard tolerances as finite-horizon approximations of these asymptotic schedules; these values are chosen on the same scale as the reported stationarity and step tolerances.

4 Convergence analysis

4.1 Basic assumptions and descent

The analysis follows the numerical active sets used in Algorithm 1. This is slightly different from the exact-active-set DCA argument because a gradient selected from an ε_k -active piece need not belong to the exact subdifferential $\partial h(x^k)$. The descent estimate therefore carries an ε_k error term. The second technical point is active-set consistency at accumulation points: a piece active at the limit can be inactive along a one-sided sequence approaching that limit, so the theorem requires the numerical active sets to capture such limiting active pieces.

Assumption 4.1. *The following conditions hold.*

1. g is convex, continuously differentiable, and has L_g -Lipschitz gradient.
2. Each ψ_i is convex and continuously differentiable.
3. The numerical active-set tolerances satisfy $\varepsilon_k \geq 0$ and $E_\varepsilon := \sum_{k=0}^{\infty} \varepsilon_k < \infty$.
4. F is bounded below and the level set $\{x : F(x) \leq F(x^0) + E_\varepsilon\}$ is compact.
5. $g + \frac{\sigma}{2} \|\cdot - x^k\|^2$ is μ -strongly convex uniformly in k for some $\mu > 0$. Equivalently, either g is strongly convex and $\sigma \geq 0$, or $\sigma > 0$ supplies the missing strong convexity.

The next lemma is the standard descent estimate for proximal DCA steps, with the additional error caused by numerical active sets; see, for example, the convergence-analysis framework in [25].

Lemma 4.2 (Numerical-active-set descent). *Under Assumption 4.1, suppose*

$$v^k \in \text{conv}\{\nabla\psi_i(x^k) : i \in \mathcal{A}_k\}, \quad \mathcal{A}_k = \{i : h(x^k) - \psi_i(x^k) \leq \varepsilon_k\},$$

and x^{k+1} solves (10). Then

$$F(x^{k+1}) \leq F(x^k) + \varepsilon_k - \frac{\mu}{2} \|x^{k+1} - x^k\|^2. \quad (11)$$

Consequently, the iterates remain in the enlarged level set from Assumption 4.1, $\sum_k \|x^{k+1} - x^k\|^2 < \infty$, and $\|x^{k+1} - x^k\| \rightarrow 0$.

Proof. Let

$$q_k(x) = g(x) - \langle v^k, x - x^k \rangle + \frac{\sigma}{2} \|x - x^k\|^2.$$

By Assumption 4.1, q_k is μ -strongly convex, and x^{k+1} is its minimizer. A μ -strongly convex function satisfies the quadratic growth inequality

$$q_k(y) \geq q_k(x^{k+1}) + \frac{\mu}{2} \|y - x^{k+1}\|^2 \quad \text{for all } y.$$

Taking $y = x^k$ and writing $s^k = x^{k+1} - x^k$ gives

$$q_k(x^{k+1}) + \frac{\mu}{2} \|s^k\|^2 \leq q_k(x^k) = g(x^k),$$

or equivalently

$$g(x^{k+1}) - \langle v^k, s^k \rangle + \frac{\sigma}{2} \|s^k\|^2 \leq g(x^k) - \frac{\mu}{2} \|s^k\|^2. \quad (12)$$

Write $v^k = \sum_{i \in \mathcal{A}_k} \alpha_i \nabla \psi_i(x^k)$, where $\alpha_i \geq 0$ and $\sum_{i \in \mathcal{A}_k} \alpha_i = 1$. Convexity of each ψ_i gives

$$h(x^{k+1}) \geq \sum_{i \in \mathcal{A}_k} \alpha_i \psi_i(x^{k+1}) \geq \sum_{i \in \mathcal{A}_k} \alpha_i \psi_i(x^k) + \langle v^k, s^k \rangle.$$

Because $i \in \mathcal{A}_k$ implies $\psi_i(x^k) \geq h(x^k) - \varepsilon_k$, we obtain

$$-h(x^{k+1}) \leq -h(x^k) + \varepsilon_k - \langle v^k, s^k \rangle.$$

Adding this inequality to (12) and dropping the nonnegative term $\frac{\sigma}{2} \|s^k\|^2$ gives (11).

Let F_{\inf} be a lower bound of F . Summing (11) from $k = 0$ to N yields

$$\frac{\mu}{2} \sum_{k=0}^N \|x^{k+1} - x^k\|^2 \leq F(x^0) - F(x^{N+1}) + \sum_{k=0}^N \varepsilon_k \leq F(x^0) - F_{\inf} + \sum_{k=0}^{\infty} \varepsilon_k.$$

The same recursion gives

$$F(x^{N+1}) \leq F(x^0) + \sum_{k=0}^N \varepsilon_k \leq F(x^0) + E_\varepsilon,$$

so the iterates remain in the compact enlarged level set. Letting $N \rightarrow \infty$ proves the summability, and therefore $\|x^{k+1} - x^k\| \rightarrow 0$. \square

4.2 Random embeddings and sampling budget

The random directions enter only through a subspace-embedding property. At iteration k , after x^k and the active set have been formed, the only vectors whose norms must be compared are linear combinations of the gradient vectors already present in the safeguard. Let

$$\mathcal{S}_k = \text{span}\{g_k, \nabla \psi_i(x^k) : i \in \mathcal{A}_k\}.$$

Thus the embedding is required on the random but finite-dimensional subspace \mathcal{S}_k , conditionally on the past, not on all of \mathbb{R}^n .

Assumption 4.3. For each k , D_k is independent of the past and satisfies, with probability at least $1 - \delta_k$,

$$(1 - \eta) \|z\| \leq \|D_k z\| \leq (1 + \eta) \|z\| \quad \text{for all } z \in \mathcal{S}_k, \quad (13)$$

where $\eta \in (0, 1)$ and $\sum_k \delta_k < \infty$.

Lemma 4.4 (Random embedding of the active span). Let $\mathcal{S} \subset \mathbb{R}^n$ be a fixed d -dimensional subspace. Let $D \in \mathbb{R}^{m \times n}$ have either independent Gaussian rows with covariance I/m , or independent rows sampled uniformly from the unit sphere and scaled by $\sqrt{n/m}$. There is a numerical constant C such that, for any $\eta \in (0, 1)$ and $\delta \in (0, 1)$, if

$$m \geq C\eta^{-2} \left(d + \log \frac{1}{\delta} \right), \quad (14)$$

then, with probability at least $1 - \delta$,

$$(1 - \eta) \|z\| \leq \|Dz\| \leq (1 + \eta) \|z\| \quad \text{for all } z \in \mathcal{S}.$$

Proof sketch. Let $U \in \mathbb{R}^{n \times d}$ have orthonormal columns spanning \mathcal{S} . For $z = Uy$, the desired estimate is equivalent to all singular values of DU lying in $[1 - \eta, 1 + \eta]$. In the Gaussian case, DU has the distribution of an $m \times d$ Gaussian matrix with entries of variance $1/m$, so standard smallest- and largest-singular-value concentration gives (14). The scaled spherical case is the corresponding isotropic bounded-row subspace embedding. These are standard oblivious subspace-embedding estimates; see [34, 14, 37]. \square

Applying Lemma 4.4 conditionally on the history justifies Assumption 4.3: at the moment D_k is drawn, \mathcal{S}_k is fixed, and the failure probability is at most δ_k . Since $\sum_k \delta_k < \infty$, the embedding failures occur only finitely often almost surely by the Borel–Cantelli lemma, which states that events with summable probabilities occur only finitely many times almost surely. Moreover $d_k := \dim(\mathcal{S}_k) \leq \min\{n, |\mathcal{A}_k| + 1\}$. Thus a sufficient per-iteration budget is

$$m_k \geq C\eta^{-2} \left(d_k + \log \frac{1}{\delta_k} \right). \quad (15)$$

The worst-case scaling is therefore linear in the ambient dimension n , not exponential in the number of possible active subsets; when the active gradients are low rank, the required number of sampled directions is governed by the active-span dimension d_k . For a finite horizon K , choosing $\delta_k = \delta/K$ gives the uniform high-probability budget $m_k = O(\eta^{-2}(d_k + \log(K/\delta)))$. For an infinite run, a summable choice such as $\delta_k = \delta/(k+1)^2$ preserves almost-sure convergence and adds only a logarithmic dependence on k .

4.3 Almost-sure directional stationarity

Assumption 4.5. *For every convergent subsequence $x^k \rightarrow \bar{x}$ and every $i \in \mathcal{A}(\bar{x})$, there is a further subsequence, not relabeled, such that $i \in \mathcal{A}_k$ for all sufficiently large k . Equivalently, no index active at an accumulation point disappears permanently from the numerical active sets along a sequence converging to that point.*

Remark 4.6 (On numerical active-set consistency). Assumption 4.5 is the only place where the analysis uses more than the exact active set at x^k . Its role is to rule out a numerical active-set artifact: an index can be active at a limiting tie \bar{x} even if it is inactive along a one-sided sequence converging to \bar{x} . Thus using exact active sets alone does not automatically imply the assumption. For any fixed positive active-set tolerance, however, the property holds on a convergent tail by continuity: if $i \in \mathcal{A}(\bar{x})$ and $x^k \rightarrow \bar{x}$, then $h(x^k) - \psi_i(x^k) \rightarrow 0$. This is the finite-horizon interpretation used in the numerical experiments. In the asymptotic theorem, where $\sum_k \varepsilon_k < \infty$, the assumption records the corresponding requirement on the tolerance schedule: every piece active at an accumulation point must be included infinitely often, or equivalently its active gap must be no larger than ε_k along a further convergent subsequence. A slower or adaptive active-set tolerance is the practical way to enforce this condition when one-sided ties are expected.

Theorem 4.7 (Directional stationarity). *Suppose Assumptions 4.1, 4.3, and 4.5 hold, and let $\tau_k \downarrow 0$. If RA-DCA uses the ε_k -active sets \mathcal{A}_k and the vertex safeguard (8)–(9), then every accumulation point of $\{x^k\}$ is directional-stationary with probability one.*

Proof. By Assumption 4.3 and the preceding Borel–Cantelli argument, the embedding event (13) fails only finitely many times with probability one. Work on this event. Lemma 4.2 gives $\|x^{k+1} - x^k\| \rightarrow 0$ and compactness gives accumulation points.

Let \bar{x} be an accumulation point and take a subsequence $x^k \rightarrow \bar{x}$ along which the embedding event holds. Suppose, for contradiction, that $R_d(\bar{x}) > 0$. Then there is an index $\bar{i} \in \mathcal{A}(\bar{x})$ such that

$$\|\nabla \psi_{\bar{i}}(\bar{x}) - \nabla g(\bar{x})\| > 0.$$

By Assumption 4.5, after passing to a further subsequence we have $\bar{i} \in \mathcal{A}_k$ for all sufficiently large k . By continuity, there is $\rho > 0$ such that

$$\left\| \nabla \psi_{\bar{i}}(x^k) - \nabla g(x^k) \right\| \geq \rho \quad \text{for all sufficiently large } k.$$

The embedding lower bound gives

$$\widehat{R}_k \geq \left\| D_k(\nabla \psi_{\bar{i}}(x^k) - \nabla g(x^k)) \right\| \geq (1 - \eta)\rho.$$

Thus, for large k , the safeguard is triggered because $\tau_k \rightarrow 0$. RA-DCA therefore uses the active vertex selected in (9),

$$v^k = \nabla \psi_{i_k}(x^k), \quad \left\| D_k(v^k - \nabla g(x^k)) \right\| = \widehat{R}_k.$$

The embedding upper bound also gives

$$\left\| v^k - \nabla g(x^k) \right\| \geq \frac{\widehat{R}_k}{1 + \eta} \geq \frac{1 - \eta}{1 + \eta} \rho.$$

For these k , x^{k+1} is the solution of (10) with this vertex. The first-order condition is

$$\nabla g(x^{k+1}) - v^k + \sigma(x^{k+1} - x^k) = 0.$$

Using the Lipschitz continuity of ∇g ,

$$\frac{1 - \eta}{1 + \eta} \rho \leq \left\| v^k - \nabla g(x^k) \right\| \leq (L_g + \sigma) \left\| x^{k+1} - x^k \right\|.$$

Thus the step length is bounded away from zero on this subsequence, which contradicts Lemma 4.2. Therefore $R_d(\bar{x}) = 0$, and Lemma 2.1 proves that \bar{x} is directional-stationary. \square

Theorem 4.7 is the main convergence result. For nonasymptotic scale, Appendix A records the corresponding worst-iterate residual bound obtained by combining the safeguard with the descent estimate. In particular, if the safeguard tolerance is of order $N^{-1/2}$ or smaller and the numerical active-set errors are summable, the best directional-stationarity residual over the last half of the first N iterations is also $O(N^{-1/2})$ on the successful embedding events. This is a stationarity-complexity estimate, not a linear convergence theorem; faster rates would require additional local regularity beyond the active-set mechanism studied here.

Remark 4.8. If the vertex safeguard is removed, the same descent proof still applies, but the limiting condition is the weaker criticality $\nabla g(\bar{x}) \in \partial h(\bar{x})$. The LP (7) should therefore be viewed as a computational stabilization and active-set compression device, not as a standalone certificate of directional stationarity. The proof of Theorem 4.7 therefore uses the LP only to generate an admissible DCA subgradient when the sampled vertex residual is already small; the logical force of the theorem is the vertex safeguard.

4.4 Finite block extensions

The single finite maximum in (2) is the basic block in a broader class of objectives with a finite sum of max terms,

$$F_b(x) = g(x) - \sum_{\ell=1}^p h_\ell(x), \quad h_\ell(x) = \max_{i \in \mathcal{I}_\ell} \psi_{\ell i}(x). \quad (16)$$

Let

$$\mathcal{A}_\ell(x) = \operatorname{argmax}_{i \in \mathcal{I}_\ell} \psi_{\ell i}(x)$$

and define the set of aggregate active vertices

$$\mathcal{V}(x) = \left\{ \sum_{\ell=1}^p \nabla \psi_{\ell i_\ell}(x) : i_\ell \in \mathcal{A}_\ell(x), \ell = 1, \dots, p \right\}. \quad (17)$$

The block directional-stationarity residual is

$$R_b(x) = \max_{v \in \mathcal{V}(x)} \|\nabla g(x) - v\|. \quad (18)$$

Since the directional derivative of the concave part is the support function of $\mathcal{V}(x)$, the same separation argument as in Lemma 2.1 gives

$$x \text{ is directional-stationary for (16)} \iff R_b(x) = 0.$$

The corresponding convex criticality residual satisfies

$$\operatorname{dist} \left(\nabla g(x), \partial \sum_{\ell=1}^p h_\ell(x) \right) \leq R_b(x),$$

and the inequality may again be strict.

For a block version of the method, let

$$\mathcal{A}_{\ell k} = \{i : h_\ell(x^k) - \psi_{\ell i}(x^k) \leq \varepsilon_{\ell k}\}$$

and let $\mathcal{V}_k^\varepsilon$ be the aggregate vertices formed from these numerical block active sets:

$$\mathcal{V}_k^\varepsilon = \left\{ \sum_{\ell=1}^p \nabla \psi_{\ell i_\ell}(x^k) : i_\ell \in \mathcal{A}_{\ell k}, \ell = 1, \dots, p \right\}.$$

The embedding subspace is

$$\mathcal{S}_k^b = \operatorname{span}\{\nabla g(x^k), v : v \in \mathcal{V}_k^\varepsilon\},$$

and the sampled residual is

$$\widehat{R}_k^b = \max_{v \in \mathcal{V}_k^\varepsilon} \left\| D_k(v - \nabla g(x^k)) \right\|. \quad (19)$$

Corollary 4.9 (Block extension). *Consider (16) and suppose the analogues of Assumptions 4.1 and 4.5 hold for the numerical block active sets. Suppose the block tolerances satisfy*

$$\sum_{k=0}^{\infty} \sum_{\ell=1}^p \varepsilon_{\ell k} < \infty.$$

Assume that D_k satisfies (13) on \mathcal{S}_k^b , with summable failure probabilities. If the block method selects an aggregate vertex attaining \widehat{R}_k^b whenever $\widehat{R}_k^b > \tau_k$, with $\tau_k \downarrow 0$, then every accumulation point is directional-stationary for (16) with probability one.

Proof. If $v^k \in \text{conv } \mathcal{V}_k^\varepsilon$, the proof of Lemma 4.2 applies block by block and gives the same descent estimate with ε_k replaced by $\sum_{\ell=1}^p \varepsilon_{\ell k}$. This includes both an aggregate vertex and a convex combination of aggregate vertices from $\mathcal{V}_k^\varepsilon$. Work on the almost-sure event on which the embedding on \mathcal{S}_k^b fails only finitely many times. If an accumulation point \bar{x} had $R_b(\bar{x}) > 0$, numerical active-set consistency would give an aggregate vertex $v^k \in \mathcal{V}_k^\varepsilon$ converging to a limiting active aggregate vertex whose distance from $\nabla g(\bar{x})$ is positive. Hence its distance from $\nabla g(x^k)$ stays bounded away from zero along a subsequence. The lower embedding bound would then keep \widehat{R}_k^b bounded away from zero, so the safeguard would select such an aggregate vertex for all large k . The first-order condition for the DCA subproblem would imply, as in Theorem 4.7, that $\|x^{k+1} - x^k\|$ is bounded away from zero on this subsequence, contradicting Lemma 4.2. Thus $R_b(\bar{x}) = 0$, which is equivalent to directional stationarity for (16). \square

The price of the block statement is that $\mathcal{V}_k^\varepsilon$ may be a Cartesian product of numerical block active sets. Thus Corollary 4.9 is most useful as a stationarity benchmark: a practical block implementation should be viewed according to how closely its active-vertex search approximates the aggregate safeguard (19). Appendix B gives a fixed-factor approximate version of this statement and records the corresponding inexact subproblem conditions. Greedy block rules without a verified approximation factor should be interpreted computationally: they test whether the same sketched active-set geometry is useful before the exact numerical aggregate safeguard is affordable.

The top- k , trimmed-regression, complementarity/binary, and QUBO experiments in Sections 6.7, 6.8, 6.9, and 6.10 use this block viewpoint. Their active-vertex search is implemented by a greedy full-space or sketched rule rather than by enumerating all aggregate vertices, so those results are reported as computational block extensions of the single-max method.

Remark 4.10 (Full-vertex scans in single and block models). For an explicit single maximum, the full-vertex residual scan is simply $\max_{i \in \mathcal{A}(x)} \|\nabla \psi_i(x) - \nabla g(x)\|$. If all active gradients are already available, this costs $O(n|\mathcal{A}(x)|)$ and is often the most direct implementation; choosing $D = I$ in (8) gives the same full-vertex scan. The situation changes for (16). An active vertex is now an aggregate $\sum_{\ell=1}^p \nabla \psi_{\ell i_\ell}(x)$, and exact full-vertex scanning requires a search over $\mathcal{A}_1(x) \times \cdots \times \mathcal{A}_p(x)$, whose size is $\prod_{\ell=1}^p |\mathcal{A}_\ell(x)|$. This combinatorial growth is the main difficulty for exact scans.

The block experiments therefore use a different object from the exact safeguard in Corollary 4.9: a greedy aggregate search. The full-space greedy reference evaluates greedy choices in the original \mathbb{R}^n space; the RA block rule performs the same type of greedy search after projecting each block gradient by D . Thus its active-set cost is tied to forming and scanning the projected block gradients, roughly $O(m \sum_{\ell} |\mathcal{A}_\ell(x)|)$ once the block gradients are available, rather than enumerating $\prod_{\ell} |\mathcal{A}_\ell(x)|$ aggregate vertices. This is why the block rule is reported as an approximate computational extension: it can track a full-space greedy aggregate choice, but it is not the exact aggregate full-vertex scan unless an additional approximation guarantee such as Appendix B is verified.

5 Implementation

The MATLAB implementation follows Algorithm 1. For a given active gradient matrix G_k and gradient g_k , the products

$$A_k = D_k G_k, \quad b_k = D_k g_k$$

are computed by one dense matrix multiply and one matrix-vector multiply. If a compatible GPU is available, the code optionally creates D_k , G_k , and g_k as `gpuArray` objects and gathers only the small projected matrices needed by the LP solver. The default LP backend is `lpSolver="gurobi"`, which calls Gurobi as a continuous LP solver. If Gurobi is unavailable, the code falls back to `linprog` and then to a projected-gradient solve of the sampled least-squares projection over the

simplex. Appendix D reports diagnostics for this LP layer: Gurobi is the fastest exact backend on the test machine, while the projected simplex method is a portable approximate fallback. The LP is skipped on iterations where the sampled vertex residual exceeds the safeguard tolerance, because the active vertex is then chosen directly. The experiment tables report CPU wall-clock times, with GPU acceleration disabled unless a table explicitly says otherwise. The separate QUBO backend diagnostic in Appendix C reports a genuinely batched GPU prototype alongside serial and batched CPU implementations.

The sketch and LP are only the active-subgradient selection layer. Once v^k has been chosen, the dominant cost in a full implementation is often the convex DCA subproblem (10). RA-DCA should therefore be paired with a solver that exploits the structure of this subproblem: closed-form updates when available, projected first-order methods for simple bound constraints, sparse linear algebra for quadratic models, or an interior-point, conic, or commercial convex-optimization solver when the model calls for it. GPU acceleration is useful in exactly this structural sense: if the subproblem solver is dominated by large matrix-vector products, batched projections, or other operations with enough arithmetic intensity to amortize data transfer, then the whole RA-DCA iteration can benefit from running those operations on a GPU. If the subproblem is small, sparse, or dominated by branching logic or factorizations better handled by a CPU solver, a specialized CPU implementation may be preferable for that case.

6 Numerical experiments

We report reproducible MATLAB experiments for several max-structured DC instances. The experiments separate three regimes: single finite maxima covered by Theorem 4.7, block sum-of-max models with combinatorial aggregate active sets, and harder penalty models where starts, the DC split, or a reference mixed-integer solver also affect the outcome. The sequence mirrors the model classes in Section 1.2; the QUBO benchmark is kept last because it adds a nonconvex quadratic term, two DC decompositions, multistart initialization, and a Gurobi MIQP reference. The tables report either averages over the stated random instances or sketches, or instancewise diagnostics when that view is more informative. Table 1 summarizes the test suite.

The tolerance sequences in Algorithm 1 should be interpreted asymptotically in the convergence theorem. The reported experiments are finite-horizon computations and use fixed small tolerances instead: $\varepsilon_k = \tau_k = 10^{-10}$ for the synthetic finite-max tests, $\varepsilon_k = \tau_k = 10^{-12}$ for the sparse support-function tests, and tie tolerances of 10^{-8} in the block penalty implementations. These fixed values do not themselves satisfy the infinite-horizon assumptions $\sum_k \varepsilon_k < \infty$ and $\tau_k \downarrow 0$; they are finite-precision approximations of the asymptotic schedules described after Algorithm 1.

Unless stated otherwise, the column “CPU s” reports average wall-clock seconds per run, measured by `tic/toc` around the solver call, on a Windows workstation with a 12th Gen Intel Core i9-12900K processor. GPU acceleration was disabled for the main CPU timing tables. The QUBO `bqp250.8` backend diagnostic is the exception: it separately reports serial CPU, batched CPU, and batched GPU timings on the same machine. The experiments use MATLAB R2023b syntax and require only base MATLAB for the fallback mode, excluding the Gurobi reference solves and the optional GPU diagnostics. The reported RA-DCA runs set `lpSolver="gurobi"` explicitly when the active-set LP backend is used.

6.1 Compared active-gradient selection rules

The single-max experiments compare the four active-gradient selection rules defined in Section 3: centered DCA, random-vertex DCA, full-vertex DCA, and RA-DCA. Once a rule has chosen v^k , all

Table 1: Overview of the numerical experiments.

test	model or data	subproblem and initialization	role in the comparison
Signed-pair max-affine	Synthetic finite maxima with $n = 50, 100, 200, 500$ and $p = 5n$ signed pairs.	Closed-form DCA step; all runs start at $x^0 = 0$.	Tests whether sampled active-set geometry finds stronger vertices.
Sketch-size study	Same signed-pair max-affine model with $n = 100, p = 500$.	One-step active-vertex screening from the degenerate start.	Measures how the number m of sampled directions affects active-vertex quality and projection cost.
Max-quadratic pieces	Signed-pair smooth pieces $\psi_i(x) = a_i^\top x + \gamma\ x\ ^2/2, \gamma = 0.25$.	Closed-form quadratic DCA step; start $x^0 = 0$.	Checks whether the same effect persists when active gradients change with the iterate.
LIBSVM support function	Signed support-function models from sparse LIBSVM data sets.	One-step max-affine DCA from $x^0 = 0$.	Tests screening on large sparse active-gradient matrices.
Top- k support function	Top- k signed support models from the same sparse LIBSVM matrices.	One-step aggregate-vertex DCA from $x^0 = 0$, using full-space and sketched greedy selection.	Tests a trimmed/sparse block active set where exact aggregate enumeration is combinatorial.
Trimmed sparse regression	Trimmed ridge least-squares models on sparse LIBSVM matrices.	One-step aggregate-vertex DCA from $w^0 = 0$; the ridge subproblem is solved by sparse linear algebra.	Tests a robust-estimation top-residual model and exposes the limits of stationarity-oriented aggregate heuristics.
LCP/MPEC penalty	Sparse synthetic row-stochastic LCP maps with $n = 100, 300, 500$.	Closed-form box projection for a sum of two-piece max blocks.	Tests greedy aggregate safeguards on nonsymmetric complementarity and binary-penalty blocks.
OR-Library QUBO	UBQP instances <i>bqp50, bqp100, and bqp250</i> , converted to minimization QUBO form.	Box QP solved by projected gradient with active-set polish and multistart.	Larger benchmark with shift/spectral DC splits and a Gurobi MIQP reference.

four methods solve the same DCA subproblem (10). Thus, “centered DCA” should not be read as the whole class of traditional DCA methods. It is one particular traditional DCA baseline with an averaged active-subgradient selection rule. The comparison is summarized in Table 2.

Table 2: Active-gradient selection rules used in the numerical experiments.

method	active-gradient selection and role
centered DCA	$v^k = \mathcal{A}_k ^{-1} \sum_{i \in \mathcal{A}_k} \nabla \psi_i(x^k)$; a traditional DCA baseline using the averaged active subgradient.
random-vertex DCA	uniformly samples one $\nabla \psi_i(x^k)$ with $i \in \mathcal{A}_k$; a single active-piece baseline.
full-vertex DCA	chooses an active gradient maximizing $\ \nabla \psi_i(x^k) - \nabla g(x^k)\ $ over $i \in \mathcal{A}_k$; an ideal full-active-set screening baseline.
RA-DCA	checks the sampled vertex residual first; if the safeguard triggers, it uses the most violating active vertex, and otherwise solves the LP for an active convex combination.

The first baseline is useful because it can stop at critical points that are not directionally stationary. The second baseline tests whether simply choosing an active vertex is enough; its performance depends on which active piece is selected. The full-vertex baseline shows what is obtained when the exact vertex residual can be scanned without sketching. RA-DCA uses sampled active-set geometry to choose between a stable convex combination step and a safeguarded active

vertex. On explicit single-max instances, the full-vertex scan is a strong benchmark and may be cheaper; RA-DCA is designed to approximate the same active-set decision when full gradients, full-space scans, or aggregate vertices are not the natural computational primitive. The full-vertex baseline is included in the single-max tests, where the scan is over the ordinary active set \mathcal{A}_k . In the block sum-of-max experiments, the corresponding exact baseline would have to scan aggregate vertices in the Cartesian product of the block active sets. For binary penalties this can mean 2^n sign patterns at a tied point, so we do not use it as a routine baseline. Instead, the same active-set idea is applied blockwise and reported as “RA-DCA block” to distinguish it from the single-max theorem and the exact aggregate-vertex safeguard in Corollary 4.9.

The active convex-combination LP (7) is not solved on every RA-DCA iteration. The implementation first evaluates the sampled vertex residual; only when that residual is below the safeguard tolerance does it solve the LP. This ordering matters because the LP is an active-gradient centering device, whereas the safeguard is the directional-stationarity test. In the main main finite-max tests, the sampled vertex residual is usually large until the method reaches a single active piece, so the LP branch is rarely on the critical path. Thus the finite-max tables should not be read as evidence that the LP itself improves the objective value; they test the vertex-first safeguard. Appendix D verifies that the LP fallback is inexpensive when it is forced or needed, and gives a near-active diagnostic where the LP prevents a spurious step caused by an ε_k -active set.

6.2 Subproblems and initialization

For the single finite-max tests in Sections 6.3–6.6, $g(x) = \frac{1}{2} \|x\|^2$. Hence, after an active subgradient $v^k \in \partial h(x^k)$ has been selected, the DCA subproblem is

$$x^{k+1} = \operatorname{argmin}_x \left\{ \frac{1}{2} \|x\|^2 - (v^k)^\top x \right\} = v^k.$$

Thus the reported differences in the affine and max-quadratic tests are entirely due to active-subgradient selection, not to numerical error in the convex subproblem solve. The signed-pair max-affine and max-quadratic tests all start from $x^0 = 0$, where the signed pairs are simultaneously active.

For the binary/complementarity and QUBO block tests, the feasible set is the box $[0, 1]^n$. The binary-complementarity subproblem has a closed-form box projection, while the QUBO relaxation gives a bound-constrained convex quadratic program. Because the only constraints are simple bounds, it is solved by a local accelerated projected-gradient routine with componentwise clipping, followed by a small active-set polish. Initial points are stated separately in the corresponding subsections because they materially affect which binary-penalty blocks are active.

6.3 Degenerate max-affine instances

We also test

$$F(x) = \frac{1}{2} \|x\|^2 - \max_{1 \leq i \leq 2p} a_i^\top x, \tag{20}$$

where the rows occur in signed pairs $a_{p+i} = -a_i$. Thus p is the number of signed pairs, and the maximum contains $2p$ affine pieces. Starting from $x^0 = 0$, all pieces are active. A centered active-subgradient DCA step again stalls, while RA-DCA uses the projected vertex residual to select a large active gradient.

Table 3 shows the targeted behaviour. The centered DCA baseline certifies only convex-combination criticality at the origin and retains a residual close to 2. The random-vertex baseline

Table 3: Results for signed-pair max-affine instances. The reported values are means over ten random instances for each dimension. Here p denotes the number of signed pairs, so the maximum has $2p$ affine pieces. CPU s is the mean CPU wall-clock time per run.

n	p	method	objective	R_d	iterations	CPU s
50	250	centered DCA	-0.0000	1.99e+00	20.0	0.00785
50	250	random-vertex DCA	-1.1887	0.00e+00	2.3	0.00117
50	250	full-vertex DCA	-1.9750	0.00e+00	2.0	0.00137
50	250	RA-DCA	-1.8246	0.00e+00	2.0	0.00347
100	500	centered DCA	-0.0000	2.00e+00	20.0	0.0115
100	500	random-vertex DCA	-0.8226	0.00e+00	2.0	0.00102
100	500	full-vertex DCA	-1.9946	0.00e+00	2.0	0.000881
100	500	RA-DCA	-1.8635	0.00e+00	2.0	0.00175
200	1000	centered DCA	-0.0000	2.00e+00	20.0	0.0855
200	1000	random-vertex DCA	-0.9551	0.00e+00	2.0	0.00489
200	1000	full-vertex DCA	-1.9983	0.00e+00	2.0	0.00555
200	1000	RA-DCA	-1.8924	0.00e+00	2.0	0.00777
500	2500	centered DCA	-0.0000	2.00e+00	20.0	0.467
500	2500	random-vertex DCA	-0.7640	0.00e+00	2.0	0.0246
500	2500	full-vertex DCA	-1.9987	0.00e+00	2.0	0.0274
500	2500	RA-DCA	-1.9383	0.00e+00	2.0	0.0288

leaves the origin and reaches $R_d = 0$, but its objective values are larger because the selected active piece is uniformly random. The full-vertex baseline gives the best objectives by scanning the complete active set and selecting the largest exact vertex residual. RA-DCA also reaches directional stationarity in about two iterations and consistently lies between random-vertex DCA and this full-active-set baseline, showing that the sketch selects substantially stronger vertices than random sampling. Because the safeguard is triggered at the degenerate start, RA-DCA skips the LP on the expensive first iteration; the largest tested max-affine case takes about 27 milliseconds per run. Figure 2 shows the same behaviour on one representative instance: the centered baseline remains flat at the initial critical point, whereas the vertex-based methods move immediately.

6.4 Effect of the number of sampled directions

For the signed-pair max-affine instances, the first RA-DCA step from the origin selects an active gradient by comparing sketched norms $\|D_k a_i\|$. The ideal active vertex is the one with largest true norm. Table 4 reports, for $n = 100$ and $p = 500$, the ratio between the true norm of the selected vertex and the best true norm, together with the fraction of trials in which this ratio is at least 0.95. Even a small number of directions gives a useful active-set summary. The projection time is the average CPU time to form $D_k G_k$.

Table 4: Effect of the number of sampled directions on active-vertex selection for signed-pair max-affine instances with $n = 100$ and $p = 500$.

m	mean ratio	success ≥ 0.95	projection ms
5	0.952	0.52	0.079
10	0.955	0.58	0.122
20	0.960	0.72	0.101
40	0.967	0.78	0.178
80	0.981	0.88	0.263
160	0.977	0.94	1.057

The results in Table 4 and Figure 3 quantify the computational role of the sketch. With only

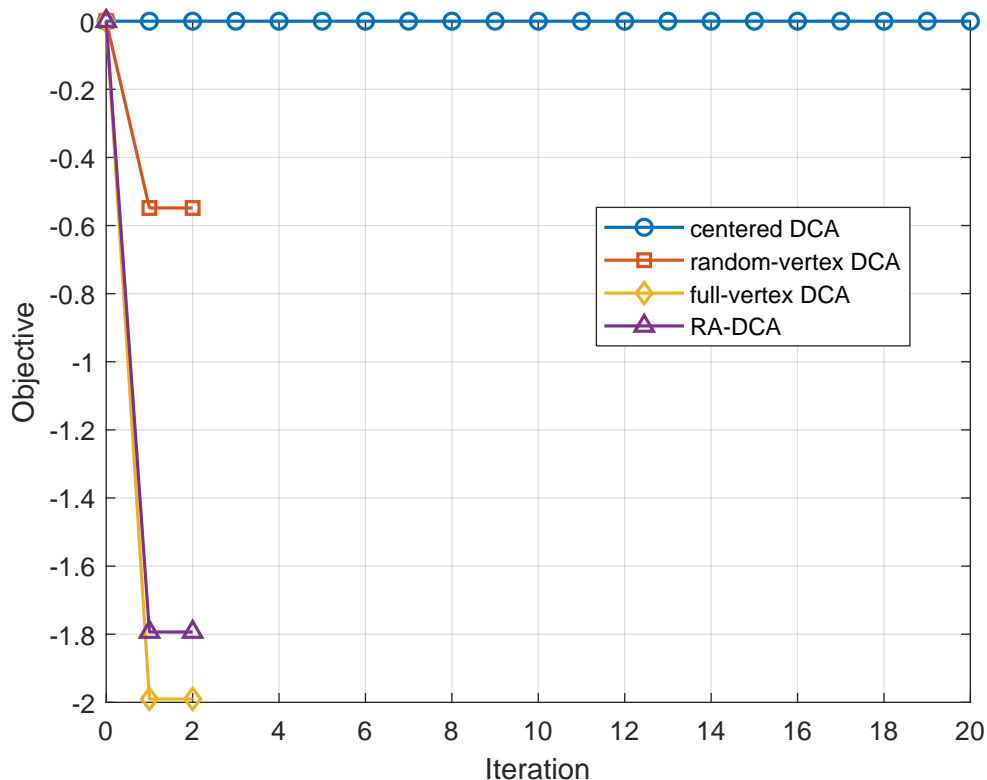


Figure 2: Objective histories on one signed-pair max-affine instance with $n = 100$ and $p = 500$. Centered DCA remains at the averaged critical point, whereas the vertex-based methods leave the origin; full-vertex DCA uses the exact active-set scan, while RA-DCA uses the sampled residual.

$m = 5$ sampled directions, the chosen vertex already has about 95% of the best active-gradient norm on average, but the least favorable trial can be substantially smaller and only about half of the trials exceed the 0.95 threshold. Increasing m improves both the average ratio and the reliability of the selected vertex, reaching a 0.94 success rate at $m = 160$. The projection remains inexpensive for these instance sizes, supporting the use of $D_k G_k$ as the dominant active-set screening operation.

6.5 Max-quadratic pieces

The smooth-piece test uses convex components

$$\psi_i(x) = a_i^\top x + \frac{\gamma}{2} \|x\|^2, \quad \gamma = 0.25,$$

with the same signed-pair construction. The full objective is

$$F(x) = \frac{1}{2} \|x\|^2 - \max_i \left(a_i^\top x + \frac{\gamma}{2} \|x\|^2 \right).$$

This keeps the subproblem simple: after an active piece is selected, the DCA update is $x^{k+1} = a_i + \gamma x^k$, or the corresponding active convex combination. The active gradients now change with the iterate, unlike the max-affine test. All runs start from $x^0 = 0$.

Table 5 shows that the same active-set effect persists when the pieces are smooth nonlinear convex functions. Centered DCA again stalls at the origin with residual nearly 2. The vertex-based

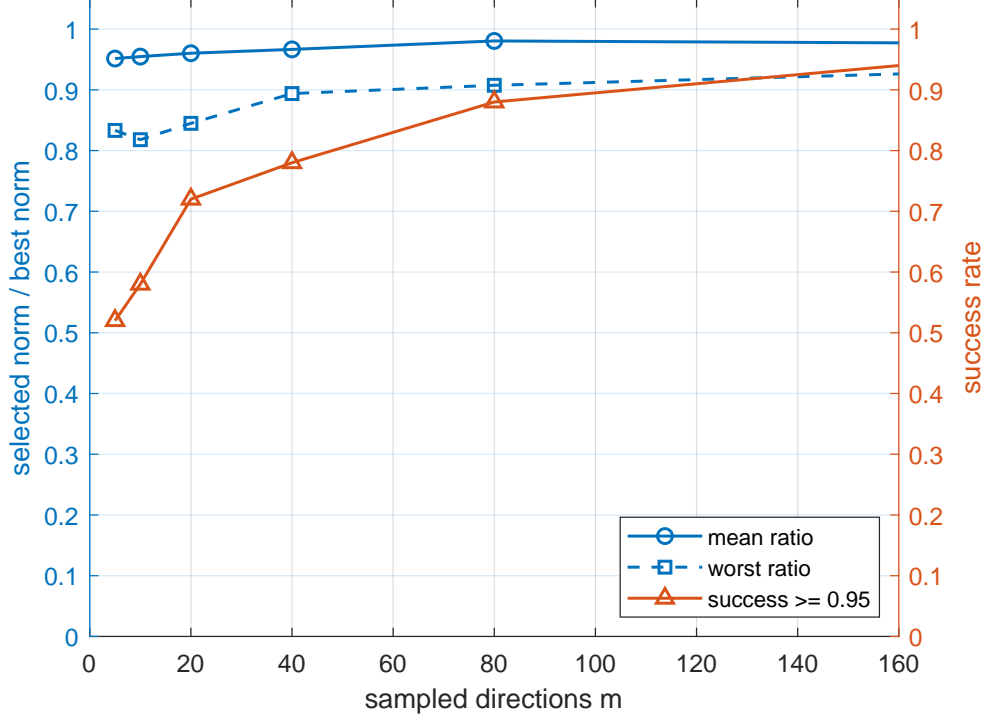


Figure 3: Sampling effect on the selected active vertex. The ratio compares the true norm of the sketched winner with the best true active-gradient norm.

Table 5: Results for signed-pair max-quadratic instances with $\gamma = 0.25$. Values are means over ten random instances for each dimension. CPU s reports per-run time.

n	p	method	objective	R_d	iterations	CPU s
50	250	centered DCA	-0.0000	1.99e+00	60.0	0.0251
50	250	random-vertex DCA	-1.4438	1.47e-11	18.3	0.00357
50	250	full-vertex DCA	-2.6333	7.23e-12	19.0	0.00413
50	250	RA-DCA	-2.4555	6.98e-12	19.0	0.0044
100	500	centered DCA	-0.0000	2.00e+00	60.0	0.0386
100	500	random-vertex DCA	-1.0063	1.72e-11	18.0	0.00348
100	500	full-vertex DCA	-2.6594	7.27e-12	19.0	0.00416
100	500	RA-DCA	-2.5012	7.04e-12	19.0	0.0044
200	1000	centered DCA	-0.0000	2.00e+00	60.0	0.252
200	1000	random-vertex DCA	-1.0372	1.25e-11	18.2	0.00781
200	1000	full-vertex DCA	-2.6644	7.27e-12	19.0	0.00973
200	1000	RA-DCA	-2.5752	7.15e-12	19.0	0.0115
500	2500	centered DCA	-0.0000	2.00e+00	60.0	1.41
500	2500	random-vertex DCA	-1.0891	1.37e-11	18.2	0.0407
500	2500	full-vertex DCA	-2.6649	7.27e-12	19.0	0.0446
500	2500	RA-DCA	-2.6241	7.22e-12	19.0	0.0453

methods all converge to residuals on the order of 10^{-11} , but the objective values separate the stationary points. Random-vertex DCA reaches stationarity quickly, yet its mean objective is much larger; for example, at $n = 100$ it ends at -1.0063 , compared with -2.5012 for RA-DCA and -2.6594 for the full-vertex reference. The separation remains at $n = 500$: RA-DCA reaches -2.6241 , close to the full-vertex value -2.6649 , while the random-vertex mean is only -1.0891 . Thus residual decrease alone is not a reliable measure of active-set quality. Figure 4 shows this on one representative instance: the random-vertex residual decreases slightly faster, but the objective

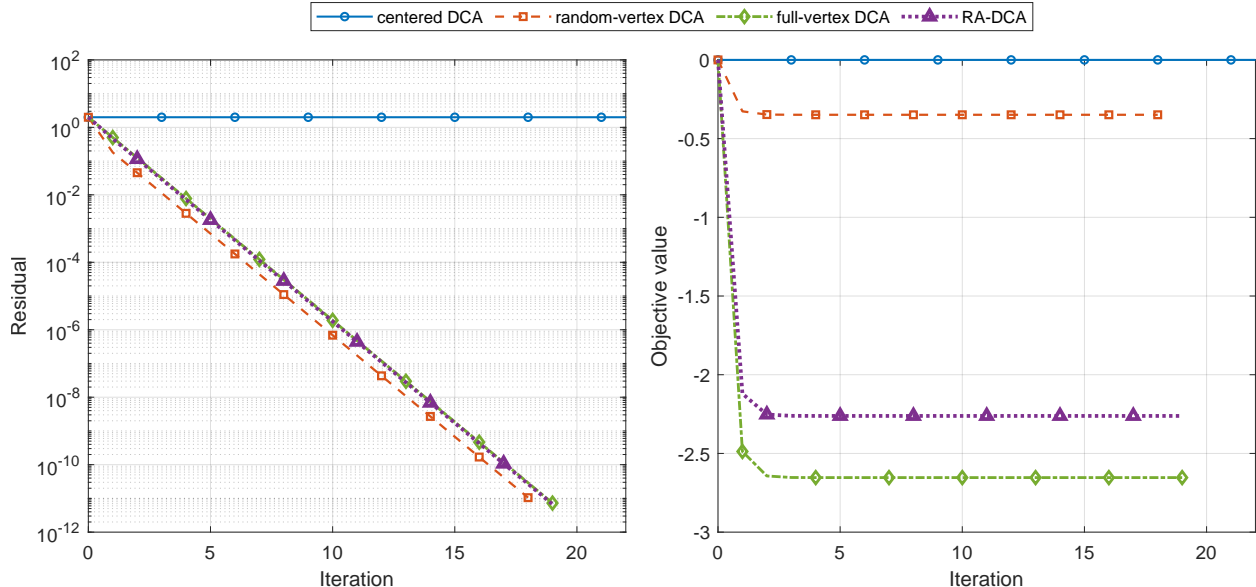


Figure 4: Residual and objective histories on one max-quadratic instance with $n = 100$ and $p = 500$. Random-vertex DCA reduces the residual fastest on this instance, but it converges to a larger objective value; RA-DCA and full-vertex DCA reach lower stationary values.

panel shows that it settles at a substantially higher stationary value. RA-DCA follows the full-vertex objective much more closely, which is the targeted effect of the sampled active-set screen.

The CPU times show that the vertex-first safeguard is important in practice: RA-DCA is now close to the full-vertex scan on these explicit synthetic active sets, while still using the same sampled residual rule that applies when a full scan is less attractive.

6.6 LIBSVM support-function benchmark

The preceding synthetic tests make the active-set geometry transparent. To check the same mechanism on larger sparse active-gradient matrices, we use three binary classification data sets from the LIBSVM collection [8]. These same matrices are also used in the top- k support and trimmed-regression tests in Sections 6.7 and 6.8. Throughout these three tests, N denotes the number of samples and n denotes the number of features, which is also the number of optimization variables in $w \in \mathbb{R}^n$. After removing zero rows, the data sizes are

data set	a8a	phishing	w8a
N	22696	11055	45546
n	123	68	300

If a_i^\top denotes one sparse data row, we form the signed support-function model

$$F(w) = \frac{1}{2} \|w\|^2 - \max_{1 \leq i \leq N} \{a_i^\top w, -a_i^\top w\}. \quad (21)$$

This is still an exact instance of (2). Starting from $w^0 = 0$, all $2N$ signed pieces are active, and the ideal full-vertex rule selects a data row with largest Euclidean norm. The RA-DCA runs use the finite-horizon direction budget (15) with $d = n$, $C = 1$, $\eta = 0.8$, and $\delta = 0.05$. The column “norm ratio” reports $\|w^1\| / \max_i \|a_i\|$, and the hit rate is the fraction of repeated runs reaching

the full-vertex objective. This benchmark measures selection quality rather than speed against the full-vertex rule. In the support-function model, the exact full-vertex score at $w^0 = 0$ reduces to a closed-form sparse row-norm scan. The row labeled “full-vertex oracle” reports this shortcut, not a generic active-set screening algorithm. RA-DCA, by contrast, keeps the same generic sampled vertex residual used in the other finite-max experiments, with all active signed rows in the candidate set; since the residual is large at the origin, the LP is skipped and the most violating sketched vertex is used directly. The test checks whether the randomized screen can recover a near-best active row from a large active set.

Table 6: LIBSVM support-function benchmark (21). The columns “samples” and “features” report N and the variable dimension n , respectively. The full-vertex oracle uses the closed-form row-norm scan available only for this support-function model. The random-vertex row averages ten random choices; the RA-DCA row uses one embedding-budget sketch. CPU s excludes data loading.

data	samples	features	method	dirs	objective	norm ratio	hit rate	CPU s
a8a	22696	123	centered DCA	–	0	0.000	0.00	0
a8a	22696	123	random-vertex DCA	–	-6.9	0.993	0.90	0.000793
a8a	22696	123	full-vertex oracle	–	-7	1.000	1.00	0.00259
a8a	22696	123	RA-DCA	198	-7	1.000	1.00	0.0714
phishing	11055	68	centered DCA	–	0	0.000	0.00	0
phishing	11055	68	random-vertex DCA	–	-0.5	1.000	1.00	0.000196
phishing	11055	68	full-vertex oracle	–	-0.5	1.000	1.00	0.00209
phishing	11055	68	RA-DCA	113	-0.5	1.000	1.00	0.0276
w8a	45546	300	centered DCA	–	0	0.000	0.00	0
w8a	45546	300	random-vertex DCA	–	-4.25	0.248	0.00	0.000659
w8a	45546	300	full-vertex oracle	–	-57	1.000	1.00	0.00456
w8a	45546	300	RA-DCA	475	-56.5	0.996	0.00	0.229

Table 6 gives a more computational stress-oriented view of the active-set rule. The centered baseline again accepts the origin even though the vertex residual is nonzero. On *a8a* and *phishing*, row norms are nearly uniform, so random vertices already perform well. The *w8a* instance is more discriminating: random vertices achieve only about one quarter of the best active-gradient norm on average, whereas RA-DCA selects a vertex with norm ratio 0.996. This improvement is not free: the sketched products use 475 sampled directions and all 91,092 active signed rows, so RA-DCA remains slower than the closed-form oracle scan. Solving the convex-combination LP before applying the safeguard would be wasteful in this case; the vertex-first implementation skips that LP and takes about 0.23 seconds on *w8a*. The oracle scan is much cheaper because this pure support-function example exposes the exact vertex scores as row norms; if this structure is available, that specialized scan is the appropriate implementation. Its role here is as an upper-quality reference. In less special max-structured models, where active gradients change with x or the exact screening score is expensive, the same table indicates the quality that the randomized screen can recover from a large active set.

6.7 Top- k support-function benchmark

The preceding support-function test has a special closed-form full-vertex scan. A top- k support model gives a sparse/trimmed block active set:

$$F_k(w) = \frac{1}{2} \|w\|^2 - \sum_{j=1}^k |(Xw)_{(j)}|, \quad (22)$$

where $|(Xw)_{(1)}| \geq \dots \geq |(Xw)_{(N)}|$ are the ordered absolute responses of the sparse LIBSVM matrix X . Equivalently,

$$\sum_{j=1}^k |(Xw)_{(j)}| = \max_{\substack{S \subseteq \{1, \dots, N\} \\ |S|=k}} \max_{s_i \in \{-1, 1\}} \sum_{i \in S} s_i a_i^\top w.$$

Thus $w^0 = 0$ has a combinatorial aggregate active set. Exact enumeration would require all signed k -subsets, so the table compares a random aggregate vertex, a greedy full-space aggregate rule, and the same greedy rule using only the sketched norms. The setting $k = 50$ is used for all three data sets, and the sketched rule uses the finite-horizon budget (15) with $d = n$, $C = 1$, $\eta = 0.8$, and $\delta = 0.05$.

Table 7: Top- k support-function benchmark (22) with $k = 50$. Here “samples” is N and “features” is the variable dimension n . The norm ratio is relative to the greedy full-space aggregate reference, not to the unavailable exact enumeration of all signed k -subsets.

data	samples	features	k	method	dirs	objective	norm ratio	CPU s
a8a	22696	123	50	centered DCA	–	0	0.000	0.00334
a8a	22696	123	50	random aggregate	–	-3.23e+03	0.156	0.00194
a8a	22696	123	50	full-space greedy	–	-1.47e+04	1.000	0.016
a8a	22696	123	50	RA sketched greedy	203	-1.49e+04	1.001	0.0923
phishing	11055	68	50	centered DCA	–	0	0.000	0.000357
phishing	11055	68	50	random aggregate	–	-234	0.139	0.000325
phishing	11055	68	50	full-space greedy	–	-1.1e+03	1.000	0.0106
phishing	11055	68	50	RA sketched greedy	118	-1.13e+03	1.031	0.0211
w8a	45546	300	50	centered DCA	–	0	0.000	0.000741
w8a	45546	300	50	random aggregate	–	-2.59e+03	0.052	0.000605
w8a	45546	300	50	full-space greedy	–	-9.11e+04	1.000	0.0399
w8a	45546	300	50	RA sketched greedy	480	-9.09e+04	0.996	0.344

Table 7 is more representative of the block difficulty than Table 6: the active set is no longer a list of single rows. Random aggregate vertices are much weaker, especially on **w8a**, where their norm ratio is only 0.052. The RA sketched greedy rule recovers essentially the same aggregate quality as the full-space greedy reference, with norm ratios 1.001, 1.031, and 0.996 on the three data sets. The ratio can exceed one because both rows are greedy heuristics for a combinatorial aggregate search; the point is that the sketch tracks the full-space greedy choice closely while avoiding explicit enumeration of all signed k -subsets.

6.8 Trimmed sparse-regression benchmark

The same sparse matrices also define a robust-estimation test. Least trimmed squares and sparse least trimmed squares are classical tools for regression with outliers [2]. With binary labels $y_i \in \{-1, 1\}$, consider

$$F_{\text{tr}}(w) = \frac{1}{2N} \|Xw - y\|^2 + \frac{\lambda}{2} \|w\|^2 - \max_{\substack{S \subseteq \{1, \dots, N\} \\ |S|=q}} \frac{1}{2N} \sum_{i \in S} (a_i^\top w - y_i)^2. \quad (23)$$

Equivalently, (23) keeps the $N - q$ smallest squared residuals and adds a ridge term. Starting from $w^0 = 0$, all squared residuals are equal to one, so every q -subset is active. Thus the first DCA step faces a combinatorial aggregate active set. For a chosen subset S^k , the active gradient of the

concave term is

$$v^k = \frac{1}{N} X_{S^k}^\top (X_{S^k} w^k - y_{S^k}),$$

and the convex subproblem is the linear system

$$\left(\frac{1}{N} X^\top X + \lambda I \right) w^{k+1} = \frac{1}{N} X^\top y + v^k.$$

The experiment uses $q = 500$, $\lambda = 10^{-2}$, and one DCA step from $w^0 = 0$. The random row averages ten random q -subsets. The full-space and sketched greedy rows approximate the aggregate residual search in the original space and the sketched space.

Table 8: Trimmed sparse-regression benchmark (23) with $q = 500$ and $\lambda = 10^{-2}$. Here “samples” is N and “features” is the variable dimension n . “Trimmed MSE” is the average squared residual over the retained $N - q$ samples.

data	samples	features	trim	method	dirs	objective	trimmed MSE	CPU s
a8a	22696	123	500	centered aggregate	–	0.2018	0.4039	0.0177
a8a	22696	123	500	random aggregate	–	0.2018	0.4039	0.00196
a8a	22696	123	500	full-space greedy	–	0.201	0.4023	0.125
a8a	22696	123	500	RA sketched greedy	207	0.2013	0.4025	0.556
phishing	11055	68	500	centered aggregate	–	0.009928	0.004196	0.00247
phishing	11055	68	500	random aggregate	–	0.009964	0.004203	0.00145
phishing	11055	68	500	full-space greedy	–	0.01235	0.01065	0.0945
phishing	11055	68	500	RA sketched greedy	121	0.01261	0.01037	0.0823
w8a	45546	300	500	centered aggregate	–	0.1525	0.2944	0.00408
w8a	45546	300	500	random aggregate	–	0.1525	0.2945	0.00361
w8a	45546	300	500	full-space greedy	–	0.1513	0.2936	0.27
w8a	45546	300	500	RA sketched greedy	484	0.1515	0.2942	2.58

Table 8 is included as a boundary test rather than as evidence of uniform improvement. On **a8a** and **w8a**, the sketched greedy rule tracks the full-space greedy rule and improves the trimmed objective relative to centered and random aggregate choices. On **phishing**, however, the same stationarity-residual heuristic gives a larger first-step objective. This does not conflict with the theory: (23) is a block sum-of-max model, and the table uses a greedy aggregate heuristic rather than the exact fixed-factor aggregate safeguard in Corollary B.1. The result marks a computational boundary. In block robust-regression models, the sketched residual can reproduce the full-space aggregate heuristic, but objective-quality improvements depend on whether that heuristic is aligned with the statistical loss.

6.9 Synthetic complementarity and binary-penalty blocks

Binary restrictions provide the simplest complementarity block:

$$x_i \in \{0, 1\} \iff 0 \leq x_i \perp 1 - x_i \geq 0 \quad (0 \leq x_i \leq 1).$$

The corresponding penalty

$$\sum_i \min\{x_i, 1 - x_i\} = \frac{n}{2} - \sum_i \max\{x_i - \frac{1}{2}, \frac{1}{2} - x_i\}$$

has exactly the two-piece max structure that produces nonstationary critical points at $x_i = 1/2$. The fully separable case is therefore a useful baseline test but is too symmetric to be a meaningful

performance benchmark: any active vertex moves a centered coordinate to a box endpoint. The reported experiment uses a less symmetric complementarity penalty.

Let $M \geq 0$ be a sparse row-stochastic matrix and $y = Mx$. On the box $0 \leq x \leq 1$, consider

$$\min_{0 \leq x \leq 1} \frac{1}{2} \|x - c\|^2 + \rho \sum_{i=1}^n \min\{x_i, y_i\}, \quad c = \frac{1}{2}\mathbf{1}, \quad \rho = 1. \quad (24)$$

This is a simple MPEC/LCP-style complementarity penalty. Since

$$\min\{x_i, y_i\} = x_i + y_i - \max\{x_i, y_i\},$$

the concave part is a sum of two-piece max blocks. For a chosen aggregate active gradient v^k , the DCA subproblem has the explicit solution

$$x^{k+1} = \Pi_{[0,1]^n} \left(c - \rho(\mathbf{1} + M^\top \mathbf{1}) + v^k \right).$$

We generate eight random sparse row-stochastic matrices for each dimension, with five nonzeros per row. The centered rule averages tied block gradients, and the random rule chooses one tied block gradient uniformly. The full-space rule uses greedy aggregate choices in \mathbb{R}^n , while RA applies the same greedy search after sketching the block gradients.

Table 9: Synthetic LCP/MPEC penalty benchmark (24). The columns “min gap” and “product gap” report $n^{-1} \sum_i \min\{x_i, (Mx)_i\}$ and $n^{-1} \sum_i |x_i(Mx)_i|$, respectively.

n	method	dirs	objective	min gap	product gap	iterations	CPU s
100	centered DCA	–	12.5	0	0	2.0	0.00211
100	random block	–	9.72	0.00907	0.00355	5.8	0.0011
100	full-space greedy	–	9.62	0.0138	0.00509	4.1	0.00185
100	RA sketched greedy	166	9.68	0.0101	0.00376	4.1	0.00307
300	centered DCA	–	37.5	0	0	2.0	0.00333
300	random block	–	29.6	0.00996	0.00391	6.9	0.00447
300	full-space greedy	–	28.2	0.013	0.00484	4.4	0.00751
300	RA sketched greedy	479	28.7	0.0113	0.00432	5.8	0.0183
500	centered DCA	–	62.5	0	0	2.0	0.0046
500	random block	–	48.8	0.0102	0.00396	7.9	0.0123
500	full-space greedy	–	47.1	0.0125	0.00475	5.1	0.0102
500	RA sketched greedy	791	48	0.0117	0.00446	5.4	0.0351

Table 9 should be read as a block-safeguard baseline test rather than a general MPEC benchmark. The centered rule quickly drives the complementarity gaps to zero by collapsing to the trivial complementary point, but this gives a larger penalty objective. The greedy aggregate rules retain a better balance with the quadratic term and lower the objective substantially. The RA sketched greedy rule stays close to the full-space greedy reference, with a modest additional cost from forming the sketch. This supports the interpretation of the QUBO and binary-penalty discussion: for block penalties, the computational question is how well a tractable aggregate search approximates the exact safeguard in Corollary B.1.

6.10 OR-Library QUBO benchmarks and Gurobi reference

We also test a less degenerate binary quadratic model. Unconstrained binary quadratic programming is a standard combinatorial benchmark class [16] and appears naturally in Boolean polynomial optimization tests [26]. The instances are thirty OR-Library UBQP problems [4], namely *bqp50.1–bqp50.10*, *bqp100.1–bqp100.10*, and *bqp250.1–bqp250.10*. The original OR-Library files are maximization instances; we use the equivalent minimization QUBO form and compare with the best-known values reported in the Biq Mac library [36]:

$$\min_{z \in \{0,1\}^n} z^\top Q z, \quad n \in \{50, 100, 250\}. \quad (25)$$

The RA-DCA-type methods are applied to the box-penalized relaxation

$$\min_{0 \leq x \leq 1} x^\top Q x + \rho \sum_{i=1}^n \min\{x_i, 1 - x_i\}, \quad \rho = 1. \quad (26)$$

For an indefinite Q , we test two DC decompositions

$$Q = Q_+ - Q_-, \quad Q_+ \succeq 0, \quad Q_- \succeq 0.$$

The first is the shift split $Q_+ = Q + \gamma I$, $Q_- = \gamma I$, with $\gamma > -\lambda_{\min}(Q)$. The second is the spectral split obtained by separating the positive and negative eigenvalues of Q . In both cases (26) becomes

$$g(x) - h(x) = x^\top Q_+ x - \left(x^\top Q_- x + \rho \sum_i \max\{x_i - \frac{1}{2}, \frac{1}{2} - x_i\} \right) + \frac{\rho n}{2}.$$

Given a block sign vector $s_i^k \in \partial \max\{x_i - \frac{1}{2}, \frac{1}{2} - x_i\}$, the DCA subproblem is the bound-constrained convex quadratic program

$$\min_{0 \leq x \leq 1} x^\top Q_+ x - \left(2Q_- x^k + \rho s^k \right)^\top x,$$

or, equivalently,

$$\min_{0 \leq x \leq 1} \frac{1}{2} x^\top H x + f^\top x, \quad H = 2Q_+, \quad f = -(2Q_- x^k + \rho s^k).$$

This problem is not separable unless Q_+ is diagonal. The inner projected-gradient iteration uses the box projection

$$x \leftarrow \Pi_{[0,1]^n} \{x - \alpha(Hx + f)\} = \min\{1, \max\{0, x - \alpha(Hx + f)\}\}.$$

The QUBO implementation therefore uses this projected-gradient iteration, with Nesterov acceleration and an active-set polish, instead of calling a generic QP solver. The Gurobi reference solve uses the Gurobi MATLAB interface when available. The DC decomposition $Q_+ - Q_-$ is computed once per instance and is not included in the reported CPU time. In particular, the spectral eigenvalue decomposition is excluded; the larger spectral runtimes in Table 10 come from the subsequent box-QP solves, since the spectral split forms dense Q_+ and Q_- , whereas the shift split preserves the sparsity of Q up to a diagonal shift. The centered method uses only $x^0 = \frac{1}{2}\mathbf{1}$ in the main OR-Library comparison. The random-vertex and RA-DCA block rows in that comparison use multistart budgets of 40, 60, and 80 for $n = 50, 100$, and 250 , respectively; the first start is $\frac{1}{2}\mathbf{1}$, and the remaining starts are independent uniform points in $[0, 1]^n$. Only RA-DCA block uses sampled directions. For

the main OR-Library rows, we set their number by the finite-horizon version of (15), using the block bound $d = n$, $C = 1$, $\eta = 0.8$, $\delta = 0.05$, and $K = 60$ times the number of starts. This gives $m = 95$, 174, and 409 for $n = 50$, 100, and 250, respectively. The constant in the embedding theorem is not optimized; this choice is a direct normalized implementation of the $m = O(n + \log(K/\delta))$ scaling. The reported objective is the original binary QUBO objective at the rounded point $z_i = \mathbf{1}_{\{x_i \geq 1/2\}}$.

In this QUBO comparison, Gurobi [13] is used only as a reference global MIQP solver for (25), with time limits of 10, 15, and 20 seconds for $n = 50$, 100, and 250, respectively. These are fixed calibration caps, chosen so that the branch-and-cut reference does not dominate the experiment. Its runtime is not directly comparable with the DCA heuristics, since it solves the binary problem rather than the penalty relaxation. Longer Gurobi runs would strengthen certificates by reducing MIP gaps, but they would not change the DCA objective values reported in Table 10. In Table 10 and Table 11 in Appendix C, ‘‘Gurobi MIP gap’’ is the relative optimality gap reported by Gurobi,

$$100 \frac{|\text{ObjBound} - \text{ObjVal}|}{|\text{ObjVal}|},$$

where ObjVal is the incumbent binary objective and ObjBound is Gurobi’s best global bound at termination. Small nonzero entries, such as 0.01%, can occur even when Gurobi reports OPTIMAL, because the certificate is closed only to the solver’s optimality tolerance; this does not mean that the incumbent objective differs from the best-known value.

Table 10: OR-Library UBQP/QUBO results on *bqp50*, *bqp100*, and *bqp250*. The gap columns report percentage gaps of the rounded binary objective relative to the best-known value. Decomposition time is excluded from CPU s. The column ‘‘dirs’’ applies only to RA-DCA block. The last column reports Gurobi’s solver optimality gap at the time limit and is therefore filled only on the Gurobi rows.

n	method	starts	dirs	mean gap %	max gap %	hit rate	CPU s	Gurobi MIP gap %
50	centered DCA (shift)	1	–	0.37	2.37	0.60	0.0124	–
	random-vertex DCA (shift)	40	–	0.00	0.00	1.00	0.172	–
	RA-DCA block (shift)	40	95	0.00	0.00	1.00	0.175	–
	centered DCA (spectral)	1	–	1.45	5.39	0.30	0.00588	–
	random-vertex DCA (spectral)	40	–	0.06	0.57	0.90	0.234	–
	RA-DCA block (spectral)	40	95	0.06	0.57	0.90	0.222	–
	Gurobi	–	–	0.00	0.00	1.00	0.017	0.00
100	centered DCA (shift)	1	–	0.48	1.88	0.50	0.00652	–
	random-vertex DCA (shift)	60	–	0.09	0.80	0.70	0.373	–
	RA-DCA block (shift)	60	174	0.07	0.65	0.80	0.379	–
	centered DCA (spectral)	1	–	1.96	4.12	0.10	0.0219	–
	random-vertex DCA (spectral)	60	–	0.14	1.10	0.70	1.33	–
	RA-DCA block (spectral)	60	174	0.14	1.00	0.80	1.32	–
	Gurobi	–	–	0.00	0.00	1.00	0.184	0.00
250	centered DCA (shift)	1	–	0.58	1.36	0.10	0.0173	–
	random-vertex DCA (shift)	80	–	0.25	0.58	0.10	1.51	–
	RA-DCA block (shift)	80	409	0.26	0.69	0.20	1.5	–
	centered DCA (spectral)	1	–	1.62	4.19	0.00	0.177	–
	random-vertex DCA (spectral)	80	–	0.48	2.26	0.10	16.8	–
	RA-DCA block (spectral)	80	409	0.46	2.25	0.10	16.8	–
	Gurobi	–	–	0.00	0.00	1.00	20.2	15.72

Table 10 shows that the QUBO behaviour is more nuanced than the fully symmetric binary-complementarity test, and the larger instances are no longer saturated by the local methods. On *bqp50*, the shift split with forty starts reaches all ten best-known values for both multistart methods. On *bqp100*, the embedding-style direction budget improves the RA-shift mean gap to 0.07%, compared with 0.09% for random-vertex DCA, and gives a 0.80 hit rate. The same budget

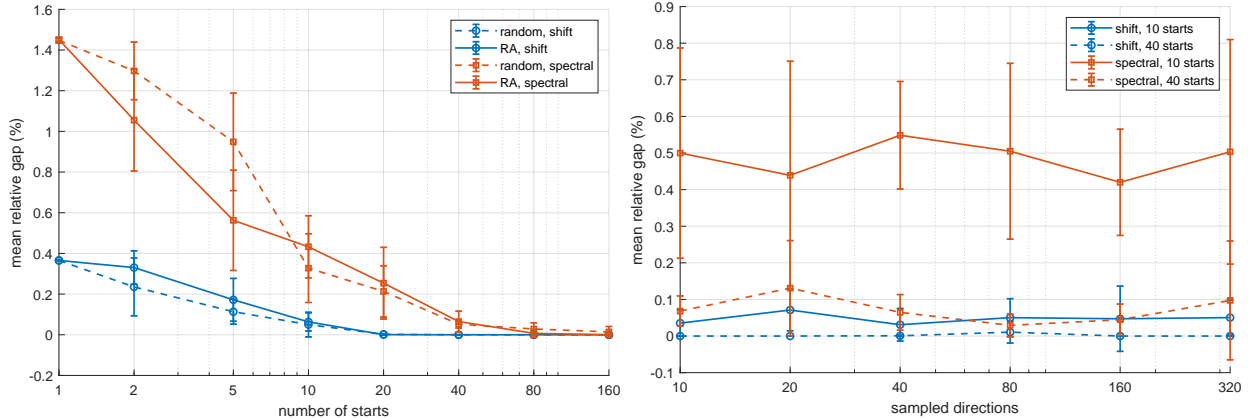


Figure 5: QUBO budget sensitivity on the OR-Library $bqp50.1$ – $bqp50.10$ instances. Left: varying the number of starts with $m = 80$ directions for RA-DCA block. Right: varying the number of sampled directions for RA-DCA block with ten and forty starts. Error bars show one standard deviation over eight random seeds.

also raises the RA-spectral hit rate to 0.80. On $bqp250$, the problem is harder and the larger direction budget is not a cure by itself: RA-shift obtains a 0.26% mean gap and a 0.20 hit rate, while random-vertex DCA has a 0.25% mean gap and a 0.10 hit rate. The spectral split is more expensive because the projected-gradient QP is harder; RA-spectral slightly improves the mean gap relative to random-vertex DCA (0.46% versus 0.48%), but not the hit rate.

Figure 5 gives a broader view of the two most natural budget parameters on the $bqp50$ group. Increasing the number of starts steadily improves both random-vertex DCA and RA-DCA block, for both decompositions. With forty starts the shift split reaches the best-known value on all ten $bqp50$ instances in all eight random repeats, while RA-DCA block with the spectral split falls below a 0.07% mean gap. Increasing the starts further continues to help the spectral split: in this sweep its mean gap drops to about 0.007% at eighty starts and to zero at 160 starts. In contrast, increasing the number of sampled directions has only a small and nonmonotone effect. The same pattern remains when the direction sweep is repeated with forty starts: the curves are lower because the multi-start budget is larger, but there is still no monotone improvement as m grows. This is expected for the binary penalty: after a random continuous start, most coordinates are not tied at $x_i = 1/2$, so the RA direction rule mainly affects the centered start and does not substitute for multi-start exploration. For QUBO, the additional budget is therefore more effective when assigned first to starts; increasing directions is a secondary tuning knob. This also explains why RA-DCA block is not uniformly dominant on QUBO. After random continuous starts, most coordinates quickly lie away from $x_i = 1/2$, and the binary penalty supplies an essentially unique block subgradient. At such iterates there is little active-set ambiguity for the randomized rule to exploit, so the quality is governed more by the start pool, the DC split, and the box-QP dynamics than by the direction sketch.

Appendix C gives the instancewise gaps, gap profiles, spectral-split tuning diagnostics, and a separate $bqp250.8$ backend diagnostic. Those tables support the same interpretation but are separated from the main text because they refine the QUBO boundary case rather than establish the finite-max active-set mechanism itself.

6.11 Computational interpretation

The single finite-max experiments are the main computational tests of the theory: the sampled vertex safeguard recovers near-full-vertex active gradients and avoids nonstationary averaged-subgradient criticality at controlled scale. The top- k support experiment gives the clearest block result, because exact aggregate enumeration is combinatorial while the sketched greedy rule closely tracks the full-space greedy reference. The remaining boundary tests show that active-set screening is not the only determinant of performance: statistical objective alignment matters in trimmed regression, and the QUBO results are strongly affected by starts and the DC decomposition. Thus the computational claim is specific: RA-DCA strengthens active-subgradient selection at nonsmooth ties or near-ties; it is not a replacement for problem-specific global or multi-start strategies.

7 Conclusions

RA-DCA is based on the following observation: for finite-max DC programs, active-gradient convex combinations are useful computationally but are not by themselves directional-stationarity certificates. The proposed method keeps the inexpensive DCA subproblem, uses randomized active-set projections to screen active vertices, and calls the convex-combination LP only as a low-residual centering fallback. The vertex safeguard is the mechanism that restores a provable directional-stationarity guarantee. The block corollary shows how the same stationarity certificate extends to finite sums of max terms when aggregate active vertices can be safeguarded.

The dominant linear algebra is a product between random directions and active gradients, making the active-set screening layer suitable for vectorized implementation and, when the surrounding subproblem solver has enough arithmetic intensity, GPU acceleration. The clearest computational evidence comes from settings where the active set itself is the bottleneck: degenerate finite maxima, sparse support-function models, and top- k aggregate selection. In these cases RA-DCA addresses the targeted stationarity gap: averaged active subgradients can certify only criticality, while a sampled vertex residual exposes the remaining directional-stationarity violation.

The mixed QUBO and trimmed-regression results also indicate the boundary of the method: when iterates spend little time at nonsmooth ties, or when starts and the DC decomposition determine the solution quality, active-set selection is secondary. For binary and QUBO-type penalty models, a natural algorithmic extension is to combine the randomized active-set selection layer with adaptive DC decompositions, penalty-continuation strategies, restart or multistart policies, and specialized bound-constrained QP solvers followed by rounding and polishing. Promising extensions also include larger block sum-of-max applications where active-set ambiguity remains central, such as MIPLIB-derived penalty instances [12], clustering models, and implicit top- k or robust-loss formulations. Other directions include acceleration techniques, such as inertial or extrapolated DCA steps [35], adaptive sampling budgets, and batched CPU/GPU kernels for large structured subproblems, as well as stochastic and variance-reduced variants [32] for empirical-risk and machine-learning models, where both data points and active max blocks may be sampled; such extensions would require new convergence analysis for stochastic active sets and inexact subproblem solves.

A Worst-Iterate Residual Bound

Proposition A.1 (Worst-iterate residual bound). *Suppose Assumptions 4.1 and 4.3 hold, and work on iterations for which the embedding event (13) holds. Let F_{\inf} be a lower bound of F ,*

$\Delta_0 = F(x^0) - F_{\text{inf}}$, $E_N = \sum_{k=0}^N \varepsilon_k$, and

$$C_\eta = \frac{(1 + \eta)(L_g + \sigma)}{1 - \eta}.$$

Then, for every such iteration k ,

$$R_d(x^k) \leq \max \left\{ \frac{\tau_k}{1 - \eta}, C_\eta \|x^{k+1} - x^k\| \right\}. \quad (27)$$

This gives the ergodic step estimate:

$$\min_{0 \leq k \leq N} \|x^{k+1} - x^k\| \leq \left(\frac{2(\Delta_0 + E_N)}{\mu(N + 1)} \right)^{1/2}. \quad (28)$$

If, in addition, τ_k is nonincreasing, then

$$\min_{\lfloor N/2 \rfloor \leq k \leq N} R_d(x^k) \leq \max \left\{ \frac{\tau_{\lfloor N/2 \rfloor}}{1 - \eta}, C_\eta \left(\frac{4(\Delta_0 + E_N)}{\mu(N + 1)} \right)^{1/2} \right\}. \quad (29)$$

Proof. Fix an iteration on which (13) holds. Since $\varepsilon_k \geq 0$, the exact active set $\mathcal{A}(x^k)$ is contained in \mathcal{A}_k . If the safeguard is not triggered, then $\widehat{R}_k \leq \tau_k$, and the lower embedding bound gives

$$(1 - \eta)R_d(x^k) \leq \widehat{R}_k \leq \tau_k.$$

If the safeguard is triggered, $v^k = \nabla \psi_{i_k}(x^k)$ and $\widehat{R}_k = \|D_k(v^k - \nabla g(x^k))\|$. Since i_k maximizes the sampled vertex residual, the lower embedding bound gives $(1 - \eta)R_d(x^k) \leq \widehat{R}_k$. The upper embedding bound and the first-order condition for (10) give

$$\widehat{R}_k \leq (1 + \eta) \|v^k - \nabla g(x^k)\| \leq (1 + \eta)(L_g + \sigma) \|x^{k+1} - x^k\|.$$

This proves (27). Inequality (28) follows by summing the numerical-active-set descent estimate (11). Applying the same summability bound to the block $\{\lfloor N/2 \rfloor, \dots, N\}$ gives an index in that block with

$$\|x^{k+1} - x^k\| \leq \left(\frac{4(\Delta_0 + E_N)}{\mu(N + 1)} \right)^{1/2}.$$

Using (27) at this index and the monotonicity of τ_k proves (29). \square

Remark A.2. Proposition A.1 is a worst-iterate complexity statement for stationarity. It shows that, if $\tau_k = O(k^{-1/2})$ or smaller and the sampling budget enforces the embedding event, the directional-stationarity residual has the same $O(k^{-1/2})$ worst-iterate decay that follows from standard descent analyses for proximal DCA, up to the accumulated numerical active-set error E_N . Under Assumption 4.1, E_N is bounded uniformly in N .

B Approximate Block Safeguards and Inexact Subproblems

Corollary B.1 (Approximate aggregate safeguard). *In the setting of Corollary 4.9, suppose that whenever $\widehat{R}_k^b > \tau_k$ the block method selects an aggregate vertex $v^k \in \mathcal{V}_k^\varepsilon$ satisfying*

$$\|D_k(v^k - \nabla g(x^k))\| \geq \theta \widehat{R}_k^b$$

for some fixed $\theta > 0$. Then every accumulation point is directional-stationary for (16) with probability one.

Proof. The proof is the same as that of Corollary 4.9. If $R_b(\bar{x}) > 0$, then along a subsequence $\widehat{R}_k^b \geq (1 - \eta)\rho$ for some $\rho > 0$. The approximate safeguard gives a selected aggregate vertex with sampled residual at least $\theta(1 - \eta)\rho$. The embedding upper bound then yields

$$\|v^k - \nabla g(x^k)\| \geq \frac{\theta(1 - \eta)}{1 + \eta}\rho,$$

and the first-order condition again forces $\|x^{k+1} - x^k\|$ to be bounded away from zero, contradicting descent. \square

Corollary B.1 states the formal boundary between theory and implementation for block heuristics. A block implementation is covered by the convergence proof if its aggregate-vertex search is an exact or fixed-factor approximation to (19). Greedy block rules without such a verified factor remain computational tests of the same active-set geometry.

The same argument allows inexact convex subproblem solves. If the computed update satisfies

$$\nabla g(x^{k+1}) - v^k + \sigma(x^{k+1} - x^k) = e^k, \quad \|e^k\| \rightarrow 0,$$

and the descent estimate remains valid up to a summable error, then the almost-sure stationarity conclusion is unchanged. For the residual bound in Proposition A.1, a relative residual $\|e^k\| \leq \kappa \|x^{k+1} - x^k\|$ simply replaces $L_g + \sigma$ by $L_g + \sigma + \kappa$ in C_η .

C Additional QUBO Diagnostics

This appendix collects QUBO diagnostics that refine the boundary-test interpretation in Section 6.10. They are not needed for the main finite-max claim, but they make clear where the QUBO behaviour is governed by starts, the DC split, and implementation backend rather than by active-set selection alone.

The gap profile gives a more cautious view than a single mean. For the shift split, random-vertex DCA and RA-DCA block have the same 0.11% mean gap, but RA-DCA block improves the fraction of instances within 0.1% of the best-known value from 0.70 to 0.77 and lowers the worst gap from 0.80% to 0.69%. For the spectral split, the two vertex-based rules are essentially tied in aggregate, which is consistent with the starts sensitivity reported in Figure 5.

The *bqp250.8* diagnostic separates search quality from backend timing: for a fixed split and start budget, all three backends use the same initial points and therefore report the same gap. The timing rows show that GPU acceleration is useful only with a genuinely batched implementation; the serial per-start GPU path is slowed by data movement and per-start kernel overhead.

D LP and Safeguard Diagnostics

This appendix records diagnostics for the active convex-combination LP (7). The first table reports how often the safeguard and LP branches are used in the finite-max experiments. A second diagnostic isolates a case where the LP branch is useful: the numerical active set contains nearly active but exactly inactive pieces. The final table compares LP backend costs. These diagnostics are separated from the main numerical section because they validate the implementation costs and clarify the LP fallback, rather than support a performance claim for an application class.

The default rows show that, on the degenerate signed-pair tests, the sampled vertex residual remains large until the method reaches a single active piece, so the LP is skipped. The LP-forced

Table 11: Instancewise QUBO gaps on the OR-Library groups *bqp50*, *bqp100*, and *bqp250*, separated by horizontal rules. Entries C-shift, R-shift, RA-shift, and RA-spec are percentage gaps relative to the best-known value; Gurobi MIP gap is the solver optimality gap at the size-dependent time limit 10, 15, or 20 seconds.

instance	best	C-shift	R-shift	RA-shift	RA-spec	Gurobi MIP gap	Gurobi s
bqp50.1	-2098	0.00	0.00	0.00	0.00	0.00	0.022
bqp50.2	-3702	0.00	0.00	0.00	0.00	0.00	0.017
bqp50.3	-4626	0.00	0.00	0.00	0.00	0.00	0.018
bqp50.4	-3544	2.37	0.00	0.00	0.00	0.00	0.014
bqp50.5	-4012	0.00	0.00	0.00	0.00	0.00	0.015
bqp50.6	-3693	0.00	0.00	0.00	0.00	0.00	0.024
bqp50.7	-4520	0.22	0.00	0.00	0.00	0.00	0.002
bqp50.8	-4216	0.00	0.00	0.00	0.57	0.00	0.018
bqp50.9	-3780	1.01	0.00	0.00	0.00	0.00	0.02
bqp50.10	-3507	0.06	0.00	0.00	0.00	0.00	0.02
bqp100.1	-7970	1.88	0.80	0.65	1.00	0.00	0.178
bqp100.2	-11036	0.45	0.00	0.07	0.00	0.00	0.188
bqp100.3	-12723	0.00	0.00	0.00	0.00	0.01	0.162
bqp100.4	-10368	0.00	0.00	0.00	0.00	0.00	0.17
bqp100.5	-9083	0.00	0.00	0.00	0.42	0.00	0.185
bqp100.6	-10210	1.07	0.08	0.00	0.00	0.00	0.243
bqp100.7	-10125	1.28	0.04	0.00	0.00	0.00	0.186
bqp100.8	-11435	0.00	0.00	0.00	0.00	0.00	0.182
bqp100.9	-11455	0.00	0.00	0.00	0.00	0.00	0.164
bqp100.10	-12565	0.14	0.00	0.00	0.00	0.01	0.179
bqp250.1	-45607	0.26	0.11	0.00	0.16	9.82	20.2
bqp250.2	-44810	1.36	0.16	0.16	0.68	14.89	20.2
bqp250.3	-49037	0.34	0.00	0.15	0.05	9.96	20.2
bqp250.4	-41274	0.55	0.27	0.09	0.36	14.60	20.2
bqp250.5	-47961	0.58	0.15	0.05	0.25	13.38	20.2
bqp250.6	-41014	0.99	0.58	0.69	0.59	21.86	20.2
bqp250.7	-46757	0.00	0.00	0.00	0.00	17.08	20.2
bqp250.8	-35726	0.56	0.56	0.56	2.25	25.38	20.2
bqp250.9	-48916	0.53	0.44	0.37	0.20	10.93	20.2
bqp250.10	-40442	0.60	0.26	0.50	0.05	19.27	20.2

rows time the convex-combination branch on the same active sets and are not used for the main performance claims here.

The following one-dimensional diagnostic shows when the LP does change the computed step. Consider

$$F(x) = \frac{1}{2}x^2 - \max\{0, c_1x - \delta, c_2x - \delta, c_3x - \delta\},$$

$$(c_1, c_2, c_3) = (0.010, 0.015, 0.020),$$

with $\delta = 3 \cdot 10^{-4}$. At $x^0 = 0$, the flat piece is the only exactly active piece and $x = 0$ is an exact directional-stationary minimizer. However, with $\varepsilon_0 = 4 \cdot 10^{-4}$, all four pieces enter the numerical active set. A vertex step can then move to an exactly stationary but larger local point generated by an inactive piece. With $\tau_0 = 2.5 \cdot 10^{-2}$ and decreasing ε_k, τ_k , the sampled residual is below the

Table 12: QUBO tuning check for RA-DCA block. Each entry averages eight independent random seeds on *bqp50.1–bqp50.10*. Decomposition time is excluded.

configuration	ρ	dirs	starts	mean gap %	std gap %	hit rate
shift, baseline	1.00	80	10	0.087	0.095	0.875
spectral, baseline	1.00	80	10	0.363	0.199	0.575
shift, larger penalty	5.00	80	10	0.084	0.086	0.838
spectral, smaller penalty	0.25	80	10	0.481	0.264	0.625
spectral, larger penalty	5.00	80	10	0.538	0.360	0.563
spectral, 20 starts	1.00	80	20	0.185	0.183	0.725
spectral, 40 starts	1.00	80	40	0.093	0.119	0.900
shift, more directions	1.00	320	10	0.034	0.042	0.888

Table 13: QUBO gap profile over all thirty OR-Library instances. The first four columns are percentage gap statistics relative to the best-known value; the last three columns report the fraction of instances whose gap is below the specified threshold.

method	mean	median	std	max	$\leq 0.1\%$	$\leq 0.5\%$	$\leq 1\%$
centered shift	0.48	0.24	0.62	2.37	0.43	0.60	0.80
random shift	0.11	0.00	0.21	0.80	0.70	0.90	1.00
RA shift	0.11	0.00	0.21	0.69	0.77	0.87	1.00
centered spectral	1.68	1.15	1.63	5.39	0.20	0.37	0.47
random spectral	0.23	0.00	0.47	2.26	0.67	0.87	0.93
RA spectral	0.22	0.00	0.46	2.25	0.67	0.83	0.93

safeguard threshold, so RA-DCA solves the LP; the LP assigns weight to the flat piece and keeps the iterate at the exact minimizer.

The backend diagnostic solves random projected active-set LPs with dimensions comparable to the sketches used in the experiments. Gurobi solves the exact ℓ_∞ LP and is the default backend. The projected fallback solves the simplex-constrained least-squares surrogate used when neither Gurobi nor `linprog` is available. The column t/t_G reports the maximum projected residual relative to the Gurobi LP value.

The projected fallback gives residuals within about 6%–11% of the Gurobi LP value in these tests, although the simple MATLAB implementation is slower for larger active sets. The reported runs therefore use Gurobi when available, while retaining the projected method as a portable fallback rather than as the preferred high-performance backend.

Statements and Declarations

Funding. The author was supported by the National Natural Science Foundation of China (Grant No. 42450242) and the Beijing Overseas High-Level Talent Program. Institutional support was provided by the Beijing Institute of Mathematical Sciences and Applications (BIMSA).

Competing interests. The author has no relevant financial or non-financial interests to disclose.

Data and code availability. The accompanying reproducibility package contains the MATLAB source code, input data, and scripts used to reproduce the reported experiments. The scripts regenerate the CSV summaries, LaTeX table fragments, and figure files used by the manuscript. The QUBO benchmark data are the OR-Library UBQP instances *bqp50*, *bqp100*, and *bqp250*, downloaded from the OR-Library raw data directory as files `bqp50.txt`, `bqp100.txt`, and `bqp250.txt`. The

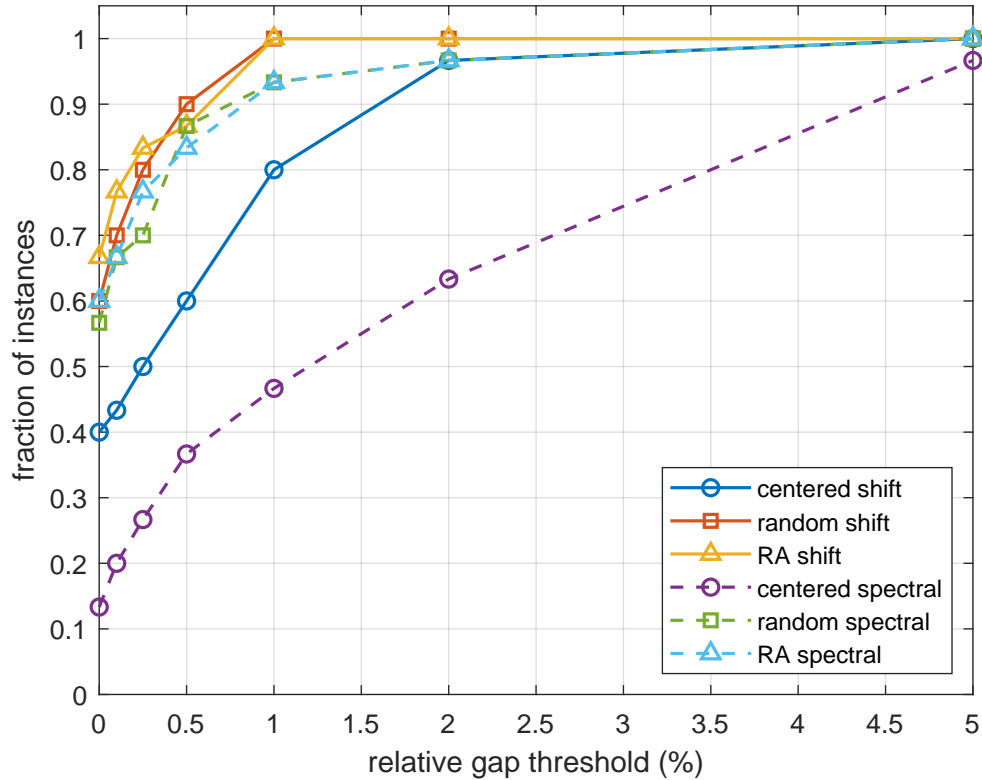


Figure 6: QUBO gap profiles over all thirty OR-Library instances. Each curve reports the fraction of instances whose rounded binary objective is within the given percentage gap from the best-known value.

best-known reference values are taken from the Biq Mac library. These values are described in Section 6.10. The real-data support-function, top- k support, and trimmed sparse-regression experiments use the LIBSVM data sets `a8a`, `phishing`, and `w8a`, downloaded from the LIBSVM binary data directory.

References

- [1] Ahmadi, A.A., Hall, G.: DC decomposition of nonconvex polynomials with algebraic techniques. *Mathematical Programming* **169**(1), 69–94 (2018). DOI 10.1007/s10107-017-1144-5
- [2] Alfons, A., Croux, C., Gelper, S.: Sparse least trimmed squares regression for analyzing high-dimensional large data sets. *The Annals of Applied Statistics* **7**(1), 226–248 (2013). DOI 10.1214/12-A0AS575
- [3] Bagirov, A.M., Taheri, S., Ugon, J.: Nonsmooth DC programming approach to the minimum sum-of-squares clustering problems. *Pattern Recognition* **53**, 12–24 (2016). DOI 10.1016/j.patcog.2015.11.011
- [4] Beasley, J.E.: OR-Library: distributing test problems by electronic mail. *Journal of the Operational Research Society* **41**(11), 1069–1072 (1990). DOI 10.1057/jors.1990.166
- [5] Ben-Tal, A., El Ghaoui, L., Nemirovski, A.: *Robust Optimization*. Princeton University Press, Princeton (2009). DOI 10.1515/9781400831050

Table 14: Starts and backend sensitivity on *bqp250.8*. The table compares serial CPU, batched CPU, and batched GPU prototypes using the same initial multistart pool. The speedup columns are relative to the matching serial CPU or batched CPU row.

split	backend	starts	gap %	time s	speedup-S	speedup-B
shift	serial CPU	20	0.560	1.69	–	–
shift	batched CPU	20	0.560	2.23	0.76	–
shift	batched GPU	20	0.560	2.48	0.68	0.90
shift	serial CPU	40	0.560	2.13	–	–
shift	batched CPU	40	0.560	1.57	1.36	–
shift	batched GPU	40	0.560	2.99	0.71	0.52
shift	serial CPU	80	0.560	4.07	–	–
shift	batched CPU	80	0.560	2.6	1.56	–
shift	batched GPU	80	0.560	3.3	1.23	0.79
shift	serial CPU	160	0.560	6.47	–	–
shift	batched CPU	160	0.560	2.09	3.10	–
shift	batched GPU	160	0.560	1.72	3.76	1.21
shift	serial CPU	256	0.498	7.13	–	–
shift	batched CPU	256	0.498	6.67	1.07	–
shift	batched GPU	256	0.498	3.47	2.06	1.92
spectral	serial CPU	20	3.101	9.13	–	–
spectral	batched CPU	20	3.101	1.05	8.68	–
spectral	batched GPU	20	3.101	3.39	2.70	0.31
spectral	serial CPU	40	2.220	15	–	–
spectral	batched CPU	40	2.220	2.34	6.43	–
spectral	batched GPU	40	2.220	3.1	4.85	0.75
spectral	serial CPU	80	2.069	30.5	–	–
spectral	batched CPU	80	2.069	1.28	23.89	–
spectral	batched GPU	80	2.069	2.08	14.65	0.61
spectral	serial CPU	160	1.360	60.1	–	–
spectral	batched CPU	160	1.360	5.98	10.05	–
spectral	batched GPU	160	1.360	3.39	17.75	1.77
spectral	serial CPU	256	1.050	96.5	–	–
spectral	batched CPU	256	1.050	2.22	43.56	–
spectral	batched GPU	256	1.050	1.73	55.67	1.28

- [6] Bertsimas, D., Brown, D.B., Caramanis, C.: Theory and applications of robust optimization. *SIAM Review* **53**(3), 464–501 (2011). DOI 10.1137/080734510
- [7] Bertsimas, D., King, A., Mazumder, R.: Best subset selection via a modern optimization lens. *The Annals of Statistics* **44**(2), 813–852 (2016). DOI 10.1214/15-AOS1388
- [8] Chang, C.C., Lin, C.J.: LIBSVM: a library for support vector machines. *ACM Transactions on Intelligent Systems and Technology* **2**(3), 27:1–27:27 (2011). DOI 10.1145/1961189.1961199. <https://www.csie.ntu.edu.tw/~cjlin/libsvmtools/datasets/>
- [9] Clarke, F.H.: *Optimization and Nonsmooth Analysis*. Wiley, New York (1983)

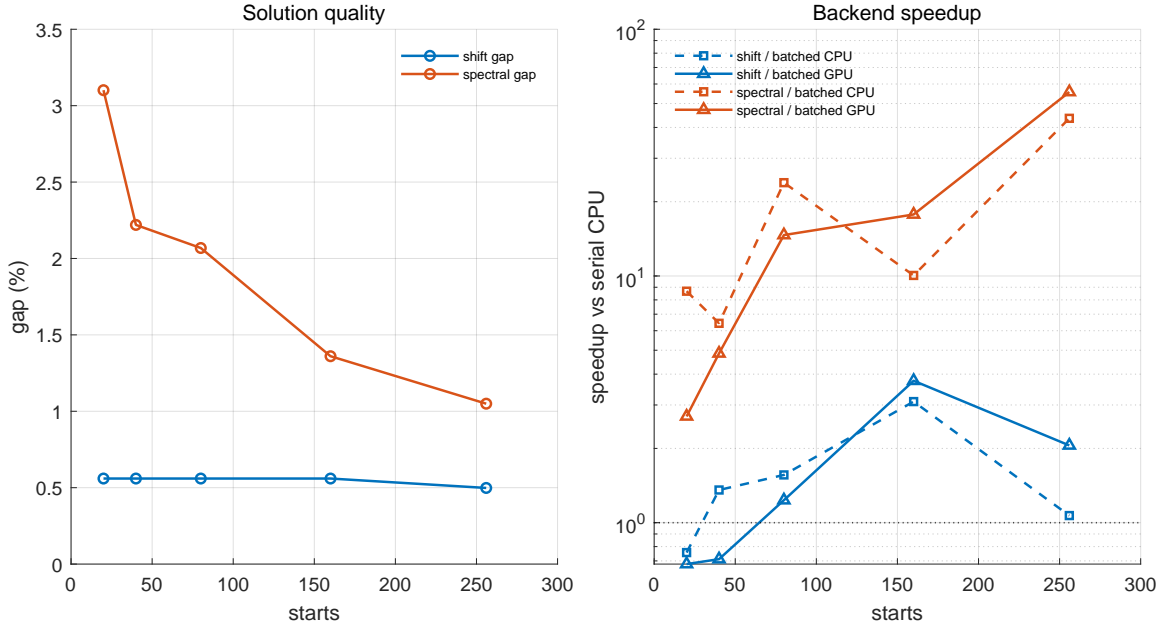


Figure 7: Starts and backend sensitivity on *bqp250.8*. Left: percentage gap versus the number of starts. Right: speedup relative to the serial CPU implementation; the horizontal line marks parity. The batched implementations solve all starts as a matrix of iterates, while the serial CPU implementation follows the default per-start loop used in the main QUBO table. For each split and start budget, all three backends receive the same initial points.

Table 15: Safeguard frequency and LP use in the finite-max RA-DCA tests. The entries are means over ten random instances. “Default” uses the parameters of the reported experiments; “LP-forced” sets the safeguard tolerance to $+\infty$ to time the convex-combination branch. “Safeguard frac.” is the fraction of iterations using an active vertex, and “LP calls” is the mean number of calls to (7) per run.

test	n	pieces	setting	iter.	safeguard frac.	LP calls	LP ms	CPU s
max-affine	100	1000	default	2.0	1.00	0.0	–	0.00904
max-affine	100	1000	LP-forced	3.1	0.65	1.1	72.78	0.0826
max-affine	500	5000	default	2.0	1.00	0.0	–	0.0272
max-affine	500	5000	LP-forced	3.0	0.67	1.0	433.74	0.462
max-quadratic	100	1000	default	18.0	1.00	0.0	–	0.00723
max-quadratic	100	1000	LP-forced	23.1	0.88	5.2	70.29	0.397
max-quadratic	500	5000	default	18.0	1.00	0.0	–	0.0386
max-quadratic	500	5000	LP-forced	19.0	0.95	1.0	429.77	0.473

- [10] Cui, Y., Pang, J.S., Sen, B.: Composite difference-max programs for modern statistical estimation problems. *SIAM Journal on Optimization* **28**(4), 3344–3374 (2018). DOI 10.1137/18M117337X
- [11] Fletcher, R., Leyffer, S., Ralph, D., Scholtes, S.: Solving mathematical programs with complementarity constraints as nonlinear programs. *Optimization Methods and Software* **19**(1), 15–40 (2004). DOI 10.1080/10556780410001654241
- [12] Gleixner, A., Hendel, G., Gamrath, G., et al.: MIPLIB 2017: data-driven compilation of the 6th

Table 16: A near-active diagnostic for the LP fallback. The exact residual is computed using the exact active set, not the initial ε_0 -active set. The LP branch prevents a spurious step caused by nearly active but exactly inactive affine pieces.

method	x	objective	exact res.	iter.	LP calls
centered eps-active	0.01125	6.33e-05	0.0112	1	0
full-vertex eps-active	0.02	0.0001	0	1	0
random eps-active	0.0114	6.56e-05	0.0059	1	0
RA-DCA LP fallback	0	0	0	1	1
RA-DCA vertex-forced	0.02	0.0001	0	2	0

Table 17: Active LP backend diagnostic. The full CSV file also reports `linprog`; the table shows the exact Gurobi LP and the projected simplex fallback.

dirs	active	solver	mean ms	median ms	t/t_G
40	500	gurobi	12.81	12.54	1.00
40	500	projected	52.65	52.38	1.11
40	2000	gurobi	79.94	75.97	1.00
40	2000	projected	980.46	963.12	1.09
80	500	gurobi	20.03	19.98	1.00
80	500	projected	50.58	49.54	1.06
80	2000	gurobi	140.23	138.23	1.00
80	2000	projected	995.66	986.14	1.09

mixed-integer programming library. *Mathematical Programming Computation* **13**(3), 443–490 (2021). DOI [10.1007/s12532-020-00194-3](https://doi.org/10.1007/s12532-020-00194-3)

- [13] Gurobi Optimization, LLC: Gurobi Optimizer Reference Manual (2026). <https://docs.gurobi.com/>
- [14] Halko, N., Martinsson, P.G., Tropp, J.A.: Finding structure with randomness: probabilistic algorithms for constructing approximate matrix decompositions. *SIAM Review* **53**(2), 217–288 (2011). DOI [10.1137/090771806](https://doi.org/10.1137/090771806)
- [15] Horst, R., Thoai, N.V.: DC programming: overview. *Journal of Optimization Theory and Applications* **103**(1), 1–43 (1999). DOI [10.1023/A:1021765131316](https://doi.org/10.1023/A:1021765131316)
- [16] Kochenberger, G., Hao, J.K., Glover, F., Lewis, M., Lü, Z., Wang, H., Wang, Y.: The unconstrained binary quadratic programming problem: a survey. *Journal of Combinatorial Optimization* **28**(1), 58–81 (2014). DOI [10.1007/s10878-014-9734-0](https://doi.org/10.1007/s10878-014-9734-0)
- [17] Le Thi, H.A., Huynh, V.N., Pham Dinh, T.: A unified approach for finding directional stationary points of DC programs (2026). ArXiv:2605.15838, <https://arxiv.org/abs/2605.15838>
- [18] Le Thi, H.A., Le, H.M., Pham Dinh, T.: New and efficient DCA based algorithms for minimum sum-of-squares clustering. *Pattern Recognition* **47**(1), 388–401 (2014). DOI [10.1016/j.patcog.2013.07.012](https://doi.org/10.1016/j.patcog.2013.07.012)
- [19] Le Thi, H.A., Pham Dinh, T.: The DC (difference of convex functions) programming and DCA revisited with DC models of real world nonconvex optimization problems. *Annals of Operations Research* **133**(1–4), 23–46 (2005). DOI [10.1007/s10479-004-5022-1](https://doi.org/10.1007/s10479-004-5022-1)
- [20] Le Thi, H.A., Pham Dinh, T.: DC programming and DCA: thirty years of developments. *Mathematical Programming* **169**(1), 5–68 (2018). DOI [10.1007/s10107-018-1235-y](https://doi.org/10.1007/s10107-018-1235-y)

- [21] Lu, Z., Zhou, Z.: Nonmonotone enhanced proximal DC algorithms for a class of structured nonsmooth DC programming. *SIAM Journal on Optimization* **29**(4), 2725–2752 (2019). DOI 10.1137/18M1214342
- [22] Lu, Z., Zhou, Z., Sun, Z.: Enhanced proximal DC algorithms with extrapolation for a class of structured nonsmooth DC minimization. *Mathematical Programming* **176**(1–2), 369–401 (2019). DOI 10.1007/s10107-018-1318-9
- [23] Luo, Z.Q., Pang, J.S., Ralph, D., Wu, S.: Exact penalization and stationarity conditions of mathematical programs with equilibrium constraints. *Mathematical Programming* **75**(1), 19–76 (1996). DOI 10.1007/BF02592205
- [24] Magnani, A., Boyd, S.P.: Convex piecewise-linear fitting. *Optimization and Engineering* **10**(1), 1–17 (2009). DOI 10.1007/s11081-008-9045-3
- [25] Niu, Y.S.: On the convergence analysis of DCA (2022). ArXiv:2211.10942, <https://arxiv.org/abs/2211.10942>
- [26] Niu, Y.S., Glowinski, R.: Discrete dynamical system approaches for boolean polynomial optimization. *Journal of Scientific Computing* **92**(2), 46 (2022). DOI 10.1007/s10915-022-01882-z
- [27] Niu, Y.S., Le Thi, H.A., Pham Dinh, T.: On difference-of-SOS and difference-of-convex-SOS decompositions for polynomials. *SIAM Journal on Optimization* **34**(2), 1852–1878 (2024). DOI 10.1137/22M1495524
- [28] Niu, Y.S., You, Y., Benammour, M.F., Wang, Y.: A parallel difference-of-convex cutting plane algorithm for mixed-binary linear programs. *Optimization* pp. 1–38 (2025). DOI 10.1080/02331934.2025.2588422
- [29] Pang, J.S., Razaviyayn, M., Alvarado, A.: Computing B-stationary points of nonsmooth DC programs. *Mathematics of Operations Research* **42**(1), 95–118 (2017). DOI 10.1287/moor.2016.0795
- [30] Pang, J.S., Tao, M.: Decomposition methods for computing directional stationary solutions of a class of nonsmooth nonconvex optimization problems. *SIAM Journal on Optimization* **28**(2), 1640–1669 (2018). DOI 10.1137/17M1110249
- [31] Pham Dinh, T., Le Thi, H.A.: Convex analysis approach to D.C. programming: theory, algorithms and applications. *Acta Mathematica Vietnamica* **22**(1), 289–355 (1997)
- [32] Reddi, S.J., Hefny, A., Sra, S., Póczos, B., Smola, A.: Stochastic variance reduction for nonconvex optimization. In: *Proceedings of The 33rd International Conference on Machine Learning, Proceedings of Machine Learning Research*, vol. 48, pp. 314–323. PMLR, New York, New York, USA (2016). <https://proceedings.mlr.press/v48/reddi16.html>
- [33] Rockafellar, R.T.: *Convex Analysis*. Princeton University Press, Princeton (1970)
- [34] Sarlóš, T.: Improved approximation algorithms for large matrices via random projections. In: *Proceedings of the 47th Annual IEEE Symposium on Foundations of Computer Science*, pp. 143–152 (2006). DOI 10.1109/F0CS.2006.37

- [35] Wen, B., Chen, X., Pong, T.K.: A proximal difference-of-convex algorithm with extrapolation. *Computational Optimization and Applications* **69**(2), 297–324 (2018). DOI 10.1007/s10589-017-9954-1
- [36] Wiegele, A.: Biq Mac Library: a collection of max-cut and quadratic 0–1 programming instances of medium size. Tech. rep., Alpen-Adria-Universität Klagenfurt (2007). <https://biqmac.aau.at/biqmaclib.html>
- [37] Woodruff, D.P.: Sketching as a tool for numerical linear algebra. *Foundations and Trends in Theoretical Computer Science* **10**(1–2), 1–157 (2014). DOI 10.1561/04000000060